energies

MDPI

Type of the Paper (Article)

Prioritizing Research for Enhancing the Technology Readiness Level of Wind Turbine Blade Leading Edge Erosion Solutions

Sara C Pryor [1,*], Rebecca J Barthelmie[2], Jacob Coburn[1], Xin Zhou[1], Marianne Rodgers[3], Heather Norton[3], M. Sergio Campobasso[4], Beatriz Mendez Lopez[5], Charlotte Hasager[6], Leon Mishnaevsky Jr.[6], and Antonios Tempelis[6]

[1] Department of Earth and Atmospheric Sciences, Cornell University, Ithaca, NY 14853, USA; sp2279@cornell.edu; jjc457@cornell.edu; xin.zhou@cornell.edu

[2] Sibley School of Mechanical and Aerospace Engineering, Cornell University, Ithaca, NY 14853, USA; rb737@cornell.edu

[3] Wind Energy Institute of Canada, Tignish, PE C0B 2B0, Canada; marianne.rodgers@weican.ca ; heather.norton@weican.ca

[4] School of Engineering, University of Lancaster, Lancaster LA1 4YW, United Kingdom; m.s.campobasso@lancaster.ac.uk

[5] National Renewable Energy Center (CENER), Sarriguren, 31621, Spain; bmendez@cener.com

[6] Department of Wind and Energy Systems, Technical University of Denmark, Roskilde, Denmark; cbha@dtu.dk; lemi@dtu.dk; atem@dtu.dk

* Correspondence: sp2279@cornell.edu; Tel.: 1-607-255-3376

Abstract: Enhanced understanding of the mechanisms responsible for wind turbine blade leading edge erosion (LEE) and advancing technology readiness level (TRL) solutions for monitoring its environmental drivers, reducing LEE, detecting LEE evolution and mitigating its impact on power production are a high priority for all wind farm owner/operators and wind turbine manufacturers. Identifying and implementing solutions has the potential to continue historical trends towards lower Levelized Cost of Energy (LCoE) from wind turbines by reducing both energy yield losses and operations and maintenance costs associated with LEE. Here we present results from the first Phenomena Identification and Ranking Tables (PIRT) assessment for wind turbine blade LEE. We document the LEE-relevant phenomena/processes that are deemed by this expert judgement assessment tool to be the highest priorities for research investment. We then discuss and summarize example research endeavors that are currently being undertaken and/or could be initiated to reduce uncertainty in the identified high priority research areas and thus enhance the TRL of solutions to mitigate/reduce LEE.

Keywords: Blades, Expert Judgement, LEE, Machine Learning, PIRT, TRL, Wind Turbine

Citation: To be added by editorial staff during production.

Academic Editor: Firstname Lastname

Received: date
Accepted: date
Published: date

Publisher's Note: MDPI stays neutral with regard to jurisdictional claims in published maps and institutional affiliations.

1. Introduction

1.1. Background and Motivation

The global wind resource greatly exceeds both current electricity demand and total primary energy supply [1]. Wind energy is a potential mechanism to reduce energy-related environmental issues (e.g. anthropogenic climate forcing [2]) and to enhance energy security [3,4]. Many countries have ambitious plans to expand both onshore and offshore wind energy installed capacity [5]. Thus, it is expected that more wind turbines will be deployed and we will become increasingly reliant on them for electricity generation.

The Levelized Cost of Energy (LCoE) in \$/MWh of electricity can be computed from

$$LCoE = \frac{\sum_{n=1}^{i}(CAPEX_n + O\&M_n)/(1+r)^n}{\sum_{n=1}^{i} AEP/(1+r)^n} \quad (1)$$

Where: CAPEX = Capital expenditures in each year (n). O&M = Operations and Maintenance costs in each year. r = annual discount rate. AEP = amount of electricity (in MWh) produced each year. i = wind turbine lifetime in years.

In locations with good wind resources, onshore wind energy has the lowest LCoE of any electricity generation type [6]. However, LCoE from onshore wind energy is no longer declining [7] and costs for offshore deployments exceed those for onshore [8].

O&M typically account for 25–30% of lifecycle LCoE from wind turbines [9]. Blades contribute > 20% of the overall cost of wind turbines [10], and blade integrity is a fundamental determinant of both O&M and power generation (AEP). An important contributing factor to wind turbine blade lifespan is leading edge erosion (LEE). LEE refers to the material loss of wind turbine blade coatings leading to exposure and ultimately loss of the laminate that provides the structure of the blade. It results primarily from materials stresses induced when hydrometeors (e.g. rain droplets or hailstones) impact on the rapidly rotating blades [11-14]. The material loss leads to roughening of the surface, reducing lift and increasing drag [15] and thus negatively impacts AEP [15-19]. LEE requiring emergency blade repair can occur within two years of installation [20], far short of the expected lifetime of 30 years [21]. O&M expenditures associated with total blade replacement for onshore wind turbines are > $200,000 and blade replacement may lead to multiple days of lost power production [22].

Wind turbines being deployed offshore are physically larger and have both longer blades and higher tip speeds than those deployed onshore [23]. This leads to higher closing velocities with falling hydrometeors, higher materials stresses [20] and thus a higher erosion rate [24,25]. Wind turbines being deployed at the South Fork wind farm off the USA east coast are GE Haliade-X 13 MW machines with blades of 107 m length each of which weighs 55 tons [26]. These wind turbines have maximum tip speeds of > 90 ms^{-1}. The 22 MW reference wind turbine that has recently been released for use in offshore research [27] has even longer blades and a rated tip-speed of 105 ms^{-1}. Manufacturing defects and damage during transportation/deployment are likely enhanced in longer blades [28,29] and even small imperfections may be important sites for initiation of LEE [29]. Thus, LEE issues may be particularly prominent offshore where O&M costs are much higher [23] and avoidance of excess maintenance is paramount to reducing LCoE. In 2018 Renew.Biz reported; The consortium behind the 630MW London Array in the UK was planning "emergency" blade repair to 140 of the project's 175 wind turbines and 'A similar repair campaign has begun at Orsted's 400MW Anholt wind farm off Denmark, where 87 of 111 ….. turbines are being fitted with rubber-like shells to fix the problem'.

LEE thus represents an important challenge to the cost-effectiveness and reliability of wind-derived electricity and there is a need to advance fundamental understanding of the processes that cause LEE and to advance effective solutions.

1.2. The Interdisciplinary Nature of LEE: Introduction to the four LEE themes

Over 40 years ago, the US National Aeronautics and Space Administration introduced "technology readiness levels" (TRLs) as a conceptual framework for measuring and articulating the maturity, or readiness for deployment, of emerging technologies. TRL assessments are usually based on a 9-point scale with higher values indicating more mature technologies and lower values indicating more nascent technologies that were in the stages of basic research, or feasibility studies [30,31].

Enhancement of the TRL for solutions to mitigate/reduce LEE requires multidisciplinary research within four linked themes (Figure 1). Theme 1 is focused on the atmospheric drivers of LEE and thus requires research primarily in the field of atmospheric science. Theme 2 is focused on detection and quantification of blade damage and thus requires research primarily within imaging and image processing plus acoustic monitoring. Theme 3 is focused on blade response/redesign/repair/protection and thus requires research primarily within the materials science field. Theme 4 is focused on detection of aerodynamic changes due to LEE and estimation of resulting power reduction and thus requires research primarily within the field of aerodynamics. All themes further require advances in computational tools and measurement technologies. An introduction to each of these themes is briefly given below.

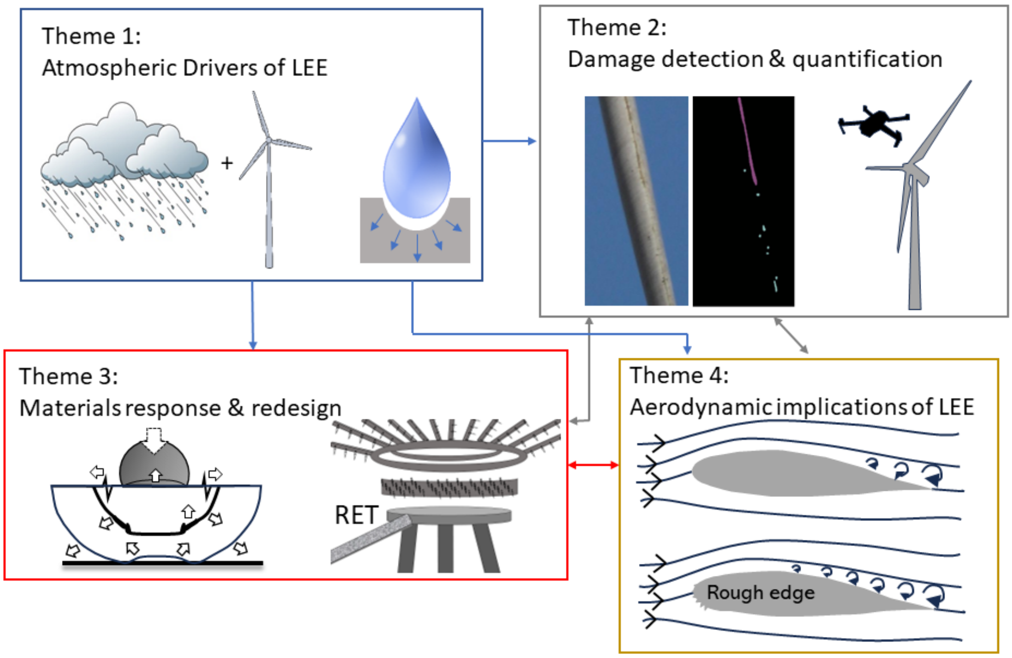

Figure 1 Schematic overview of the four LEE themes. RET = Rain Erosion Tester.

Theme 1. Atmospheric drivers of LEE

The amount of kinetic energy transferred into the blade from an ensemble of falling hydrometeors and the materials response is dictated by the closing velocity (v_c) between the falling hydrometeor(s) and the rotating blades, plus the number, diameter (D) and phase of hydrometeors (i.e., hailstones, graupel or rain droplets). The impact force and the kinetic energy transferred into the coating scales with the hydrometeor mass and closing velocity squared [32]. Larger diameter drops may be of greater importance in dictating the kinetic energy transfer to the blades and hence the duration of the incubation period (i.e. period prior to material loss, see details below) [14,33] while smaller drops may be more critical in the transition and steady-state progression [34]. The Waterhammer equation describes the pressure exerted on a coating by the impact as a function of closing velocity [32,35,36]. For v_c = 80 ms^{-1} a single 2 mm diameter rain droplet may exert a pressure of up to 120 MPa on the blade surface [32]. Hydrometeor phase is of importance because the materials response to hail (ice) exceeds that due to collisions with rain (liquid) droplets [32,37-40]. As few as five hailstone impacts (D of 15 and 20 mm) at $v_c \geq 110$ ms^{-1} can cause damage to a glass fibre reinforced plastic composite [41]. Thus, prediction of LEE requires accurate and consistent descriptions of hydroclimate conditions, including precipitation intensity, phase and hydrometeor size distributions (HSD) from measurements and models across the wide range of environments in which wind turbines are or will be deployed. However, as discussed in detail below, best practice for the selection and operation of precipitation sensors within the context of LEE has not yet been advanced [14] and numerical models exhibit only partial fidelity for precipitation rate and phase and most simulations do not explicitly simulate or output HSD.

A hierarchy of models have been generated to translate from precipitation intensity/HSD and closing velocities to provide estimates of potential erosion. First-order erosion models rely on the volume (or depth) of impinged water without explicit consideration of hydrometeor size and/or phase [24]. Alternatively, VN curves (velocity-number of impacts to failure, see 'Materials response') derived from rain erosion testers can be used to articulate functions that describe the number of impacts at a given closing velocity for a given hydrometeor diameter required for initiation of coating damage and that can be used (with caution) to extend beyond the measured range of closing velocities. For example, assuming all hydrometeors have an effective diameter of 0.76 mm, the accumulated distance to failure (ADF) of the coating is given by;

$$ADF = \sum_{i=1}^{j} \frac{V_{tip} \cdot I \cdot \Delta t / v_f}{H_0 \cdot \left(\frac{v_c}{V_0}\right)^m} \quad (2)$$

Where V_0 is 1 ms^{-1}, v_c is the closing velocity between the hydrometeor and blade, v_f is the hydrometeor fall velocity (ms^{-1}), Δt is the time interval (s) for the specification of the tip speed and precipitation intensity (I, in ms^{-1}). H_0 and m are fitting parameters that are specific to the coating material tested but for one coating and D = 0.76, these fitting parameters are 2.85×10^{22} m and -10.5, respectively [42]. The summation is over all time periods; i=1 to j. Thus, the challenge is to specify a representative effective diameter to characterize precipitation that falls from stratiform and cumulus clouds and over a wide range of intensity ranges [43]. More mechanistic models require greater specificity in terms of the HSD/phase and range of fall velocities and are described below in Theme 3.

Less is known regarding the possible contribution of other meteorological variables to LEE. Prolonged exposure to radiation within the visible range, and particularly UV-A (wavelengths (λ) = 320 and 400 nm), may lead to degradation of polyurethane coatings [32,44]. Theoretical and experimental work has also indicated that low temperatures degrade the erosion performance of polyurethane protective leading-edge coatings [45]. Thermal cycling (expansion and contraction of the blades) is an important source of materials wear [46]. Other plausible meteorological co-stressors include impacts from aerosols (e.g. wind-blown dust/sand [47,48]) and ice accretion on blades [49].

Theme 2. Damage detection and quantification

LEE pattern categorization frequently employs five classes with Class 1 "small pinholes" exhibiting erosion depth of 0.1-0.2 mm, average feature damage of 2 mm and approximate cord coverage of 3% [17]. Even Class 1 LEE may result in AEP loss. Early detection and close monitoring of damage progress can help optimize mitigation strategies and identify appropriate maintenance actions (patching and minor repair to full scale blade removal) [50-53].

Current techniques for real-time wind turbine blade damage detection [54,55] include; vibration-based techniques [56], ultrasound scanning techniques [57], acoustic emission monitoring [58], and machine vision image or video processing [59]. Three out of four of these LEE detection methods (acoustic emission, ultrasound, vibration-based techniques) require the use of physical sensors placed along the blade or near the wind turbine, which can be costly and vulnerable to damage in extreme meteorological conditions [60]. Image processing methods can be used to assess blade conditions from 2-D and 3-D images or videos captured by instrumentation deployed on unmanned aerial vehicles (UAVs) [61] or taken by technicians [62]. However, as discussed below, the fidelity of different damage detection methods has not been fully quantified.

Theme 3. Materials response

Wind turbine blades are made of composites (e.g. epoxy or polyester, with reinforcing glass or carbon fibers) [63] coated to protect them by distributing and absorbing energy from hydrometeor and other impacts [64]. Defects such as air bubbles in these coatings have a critical impact on crack initialization [65] and re-emphasizes the importance of wind turbine blade manufacturing quality in dictating erosion rates.

Erosion mechanics comprises an incubation period during which no damage is observed but microstructural material changes can generate nucleation sites for subsequent material removal. Material removal commences when a threshold level of accumulated impacts is reached [66]. This is followed by a period during which additional impacts lead to observable damage as stress waves propagate from impact locations. This leads to growth of pits/cracks and an increase in material loss [67-69]. The number of impacts required to reach the threshold at which material failure becomes evident is thus a nonlinear function of the number, magnitude and phase of the hydrometeors and hydrometeor closing velocity plus the material strength [70].

Whirling-Arm Rain ERosion testers (WARERs, or more simply Rain Erosion Testers, RET) artificially simulate the erosion process by spinning a sample of the blade, often with a leading edge protection applied, at very high speeds and bombarding the sample with liquid droplets (of a confined droplet diameter range) supplied via needles [71]. These experiments can be used to develop VN curves and thus to derive empirical coefficients for use in Equation (2). However, the range of closing velocities sampled and used to derive the fitting parameters m and H_0 specified below Equation (2) for hydrometeor D of 0.76 mm are 90 to 150 ms^{-1} and thus exceed many of those that will occur.

Alternatively, a range of modeling techniques have been advanced to simulate the process of material stresses that lead to LEE as a function of hydrometeor size distribution and closing velocity [68,70,72]. The simplest is the Springer model [73,74] combined with Miner's rule to integrate across all hydrometeor diameters to quantify the accumulated distance to failure (ADF) [66,75]. However, these simple engineering models of LEE include multiple coefficients/assumptions that limit the robustness of lifetime estimates and when invoking Miner's rule, assume damage is linearly accumulated.

Theme 4. Aerodynamic implications of LEE

A smooth leading edge reduces turbulence and drag, optimizing the lift-to-drag ratio of a wind turbine blade. The outer part of the blade (towards the tip) produces most of the energy and experiences the highest relative wind speeds. Thus, the leading edge towards the blade tip is both the most vulnerable to roughening by material loss and is also where reducing lift/increasing drag maximizes negative impacts on AEP. Maximum lift force on blades has been modeled to be reduced for damage associated with roughness heights of 0.11 mm for a rotor with a 175 m diameter [16]. Erosion classes 3 to 5 (large patches of missing coating, erosion of laminate and complete loss of laminate, respectively), are associated with AEP reductions of 1-5% [76]. Recent reports found LEE-induced AEP losses from onshore wind turbines after only 1-3 years [77] but there is a paucity of data regarding underlying blade LEE topologies. Damage location on the blade is known to play a critical role in alteration of the aerodynamic behavior and so there are clear links between themes 2 and 4 [78].

The Simplified Aerodynamic Loss Tool (SALT) model [79] can be used to illustrate the predicted effect of erosion on the power coefficient (C_P) and AEP loss relative to a clean or undamaged blades, while acknowledging it omits many of the details of more complex models [80]. Within SALT damage is specified in 2% increments over the outer 70% of the blade (location r as a fraction of blade radius R) using a five-level categorization. Category a is undamaged, and lift-to-drag ratio (C_l/C_d) is estimated as 1. Category e represents the most severe damage deeper than 0.3% of the blade chord and C_l/C_d = 0.3. For the IEA 15 MW reference wind turbine [81] and a hub-height wind speed of 10 ms^{-1}, C_P for an entirely undamaged blade is ~ 0.4551 reducing to ~ 0.2907 for category e damage. C_P correction factors (multipliers to C_P) are shown as a function of r/R in Figure 2a for wind speed of 10 ms^{-1}. The impact of roughening of the leading edge on blade lift and drag and power production is a non-linear function of inflow wind speed and is specifically important at below rated wind speeds (Figure 2b) and also depends on turbulence intensity [19]. Thus, the AEP loss is dependent on the site wind climate. Assuming a Weibull distribution of hub-height wind speeds for a typical US Central Plains site [14], AEP loss for different erosion levels along the outer 70% of the blade is shown in Figure 2c. While this analysis is useful for illustrative purposes, uniform damage is unlikely to occur across such large areas of a blade thus the AEP loss estimates greatly exceed those that are likely to be observed. Further, attribution of any loss in blade performance to any specific cause (e.g. LEE, gearbox wear-and-tear, soiling of blades) is very challenging [82,83] particularly in operating wind farms.

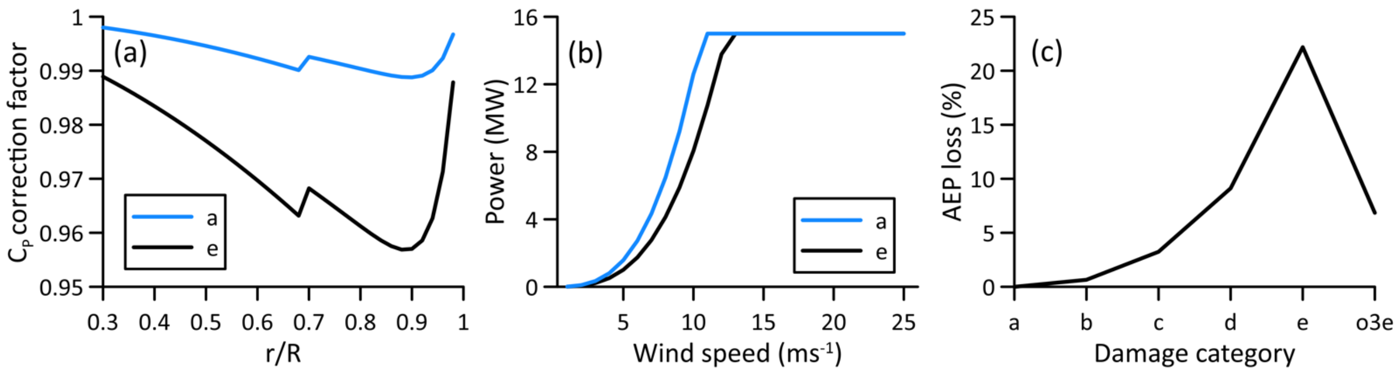

Figure 2 Results from the SALT model for (a) C_P correction factors as a function of distance along the blade for a clean blade (shown by the blue line, Category a damage) and substantial damage (shown by the black line, Category e damage) along the outer two thirds of the blade for a hub-height wind speed of 10 ms^{-1} for the IEA 15 MW reference wind turbine. (b) Power curves (power generation as a function of hub-height wind speed) for the IEA 15 MW reference wind turbine for a clean blade (Category a damage) and a damaged blade (Category e damage). (c) AEP loss for damage categories a to e and o3e (level 3 damage only for the outer 1/3 of the blade) for the IEA 15 MW reference wind turbine and the Weibull distributed wind speeds from a US Southern Great Plains site [14].

Optimizing O&M as LEE progresses for cost-effectiveness requires not only accurate damage assessment but also robust, quantitative understanding of the effect of LEE on blade aerodynamics. For example, if the damage is minor pitting without material losses, the aerodynamic efficiency may only be slightly lower than its design, and potentially even only impacting the aerodynamics at some tip speed ratios. In this case, unless the damage is likely to propagate it may be more cost effective to wait rather than to order repairs. On the other hand, if material damage has penetrated beyond the blade coating, even a small gouge may potentially leave open the possibility of further material loss and extensive delamination impacting not only the aerodynamics but necessitating costly on-site repairs.

1.3 Possible Solutions for Leading Edge Erosion

Fundamentally, efforts to reduce LEE can be placed into two classes:

- Enhanced blade resilience. This may be achieved by blade redesign and/or use of improved materials (e.g. more energy consuming coatings) [84,85], improved manufacture and/or use of leading edge protection (LEP) products. A range of LEP products are available including: (1) In-mould application of a gelcoat (e.g. epoxy) during blade manufacture or co-bonding to an erosion shield (rigid/semi rigid covers). (2) Post-mould application of flexible coatings (e.g. polyurethane [86]) using sprayers/rollers or flexible tapes [87] or thermoplastic erosion shields [88]. Details of the relative merits of these solutions, including their durability have been previously reviewed [20,89,90]. Best practice for the optimal length of LEP from the tip of the blade is being investigated [91] as is the optimal thickness of application [92]. All protective solutions incur additional costs and reductions in aerodynamic performance and AEP. For example, some research has reported 2-3% AEP losses from LEP tapes [87,93]. Further, some post-mould LEP products are challenging to apply (see below, section 3.4) and/or lack durability [94].

- Operation of wind turbines in a manner to reduce materials stresses. Specifically, use of erosion safe mode [11] wherein wind turbine operation is modified during highly erosive periods to reduce blade rotational speed, thus sacrificing AEP to elongate blade lifetime [95].

Both classes of solution require detailed assessment of site conditions regarding likely severity of LEE since the incubation, transition and steady-state progression of damage on the leading edge differs as a function of precipitation climate and possibly other operating conditions [16]. Quantitative comparison of overall cost effectiveness requires detailed information regarding (i) AEP loss from LEE, LEP application (including down-time if LEP is applied post commissioning) and/or adoption of erosion safe mode. (ii) Cost of LEP measures and expense of deployment [96] and robust economic/financial information such as the spot market price for electricity [97]. Ultimately an optimal solution is likely to be one which maximize revenues over a specific period of time for a given wind farm [98]. Consideration of either solution type for a given situation demands robust knowledge of processes/phenomena in each of the four themes described above. Thus, the issue confronting the wind energy industry is how to prioritize research to reduce uncertainty and increase confidence for wind farm owners/operators and enhance the TRL for LEE mitigation.

1.4 Objectives of this Work

Our goal is to map priorities for LEE research that can enhance the technology readiness levels for LEE solutions such as those described in section 1.3, and thus aid in reducing the LCoE from wind turbines. To achieve this goal we undertook, and herein present, the first Phenomena Identification and Ranking Tables (PIRT) assessment for wind turbine blade LEE (section 2). Following presentation of the PIRT analysis, we discuss research required and/or being conducted to address the highest priority research needs identified during the PIRT process and that is necessary to enhanced TRL of LEE solutions (section 3). We conclude in section 4 by describing next steps.

2. PIRT

The PIRT process is a systematic way of gathering information regarding processes on a specific concept and ranking their importance to meet some decision-making objective such as prioritization of research activities to enhance the TRL. PIRT has been widely applied within, for example, nuclear safety [96,99,100], but is gaining traction in other disciplines [101].

A schematic workflow of the PIRT process as applied in this research is given in Figure 3. Steps 1 and 2 require identification of a topic of interest and then articulation of the PIRT objective(s). To aid in structuring the PIRT by thematically clustering of processes/phenomena, in Step 3 four LEE themes were articulated (section 1). The PIRT analysis then proceeded by polling experts to identify key phenomena in each of those LEE themes, acknowledging that some phenomena cross the thematic boundaries. Following best practice in prior PIRT analyses [96], once each of the processes/phenomena were identified then domain experts were asked to provide for each a ranking of 'High', 'Medium' or 'Low' priority. To derive a mean ranking and the standard deviation (SD) across respondents, rankings of 'high' were allocated 1 point, medium as 0.5 and low as 0. As an example, the need for hydrometeor size distributions (HSD) (jointly with wind speeds) to inform LEE assessment was given a mean ranking of 0.86 and the standard deviation is 0.32 (Table 1). These rankings are because > 80% of respondents gave a ranking of high, and approximately 10% gave a ranking of either medium or low.

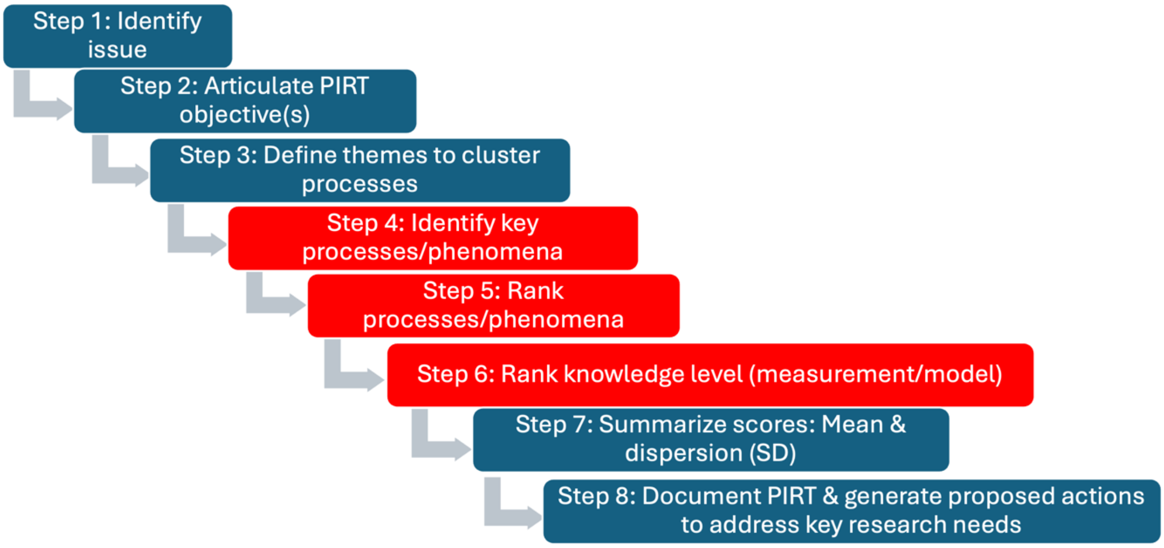

Figure 3 Workflow of the PIRT process. Steps in red indicate solicitation of expert judgements.

Table 1. PIRT analysis results. Column 1: Processes/phenomena of interest. Columns 2 and 3: Mean (Mean) ranking and the standard deviation (SD) of the rankings across respondents. Expert judgement evaluation of the knowledge regarding each process/phenomenon as translated into state-of-the-art measurements (columns 4 and 5) and modeling (columns 6 and 7). Items in black have high importance (mean > 0.8) and process-level understanding has been well-translated to measurement technologies and/or modeling (mean > 0.5). Process/phenomena in red have high-importance (mean > 0.8) but process-level knowledge is lacking and/or translation of that knowledge to measurement and modeling capabilities is poor (mean < 0.5) and thus are defined as Tier 1 for research. Items in blue are Tier-2 priorities for research; moderate importance (0.5 < mean < 0.8) and process-level knowledge and translation to models and measurements incomplete (mean < 0.6). Items in green have importance level scores (mean < 0.5). Note: Process/phenomena are listed in the order in which they were presented to the respondents to avoid confusion that the rank order of importance is systematically a function of the row number in the PIRT.

	Process/Phenomena Importance Level		Measurement		Modeling	
Theme 1: Atmospheric drivers	Mean	SD	Mean	SD	Mean	SD
Hub-height wind speeds: existing wind farms	0.92	0.19	1	0	0.73	0.26
Hub-height wind speeds: prospective wind farms	0.91	0.2	0.82	0.25	0.68	0.25
Hydrometeor size distribution	0.86	0.32	0.27	0.41	0.2	0.26
Hydrometeor phase (rain/hail/other)	0.91	0.3	0.36	0.39	0.14	0.23
Hydrometeor fall velocities	0.58	0.36	0.41	0.38	0.32	0.34
Impinged water (blade capture efficiency as a function of droplet diameter)	0.55	0.44	0.15	0.34	0.1	0.21
Real-time data for 'erosion safe mode'	0.68	0.25	0.18	0.34	0.46	0.33
Space/time variability in hydroclimate conditions	0.64	0.23	0.59	0.2	0.59	0.2
Non-hydrometeor weathering stressors (e.g. UV radiation, icing, thermal expansion, aerosols (incl. dust & pollution))	0.55	0.27	0.18	0.25	0.27	0.34
Reanalysis/gridded product data quality	0.44	0.17	0.67	0.25	0.81	0.26
Theme 2: Damage detection and quantification	Mean	SD	Mean	SD	Mean	SD
Availability of blade images & methods to quantify damage	0.83	0.25	0.54	0.33	0.5	0.33
Damage characterization from varying image types & methods to translate to damage classification	0.88	0.23	0.58	0.29	0.44	0.3
Methods for 3-D characterization of damage morphology & rate of progression	0.71	0.26	0.25	0.26	0.18	0.25
Translating water impingement to materials loss/stress (e.g. metrics: Kinetic Energy, Springer-ADF, VN curves)	0.86	0.23	0.27	0.26	0.36	0.23

Quantification of materials loss	0.71	0.26	0.5	0.39	0.27	0.26
Quantification of equivalent surface roughness for aerodynamic loss	0.75	0.26	0.41	0.3	0.45	0.27
Microplastic loss for environmental impacts	0.5	0.21	0.21	0.26	0.27	0.26
Theme 3: Materials response	Mean	SD	Mean	SD	Mean	SD
Rain erosion tester reliability & reproducibility	0.92	0.19	0.59	0.3	0.4	0.21
Rain erosion tester representation of atmospheric conditions: hydrometeors: phase (e.g. rain and hail), size distributions & collision velocities	0.83	0.25	0.5	0.33	0.28	0.26
Rain erosion tester representation of atmospheric conditions: flow field (e.g. impact velocities)	0.71	0.33	0.45	0.28	0.28	0.36
Methodologies to translate lab experimental data (incl. rain erosion tester) to field conditions & failure modes	0.88	0.23	0.35	0.24	0.3	0.26
Damping and energy dissipation properties of LEPs/coatings (single/multilayer)	0.67	0.25	0.32	0.25	0.45	0.16
Linking mechanical and viscoelastic properties to failure mechanisms/modes	0.73	0.26	0.32	0.25	0.4	0.32
Coating adhesion & mechanics of multi-layer materials	0.75	0.26	0.45	0.44	0.55	0.28
Material response to non-hydrometeor weathering stressors (e.g. UV radiation, icing, thermal expansion, aerosols (incl. dust))	0.64	0.23	0.36	0.32	0.35	0.24
Theme 4: Aerodynamic implications of LEE	Mean	SD	Mean	SD	Mean	SD
Quantification of damage and surface roughness progression through time	0.95	0.16	0.4	0.32	0.45	0.28
Attribution of AEP loss to LEE (via effective surface roughness)	0.88	0.23	0.35	0.34	0.5	0.24
Attribution of AEP loss to application of LEP measures	0.75	0.26	0.4	0.39	0.55	0.28
Quantifying evolution of power curve through time (incl. post deployment)	0.75	0.26	0.3	0.42	0.3	0.42
Optimization of damage repair solution/timing	0.9	0.21	0.35	0.34	0.5	0.33

The second component of PIRT analyses (Step 6) is to evaluate the state of knowledge with respect to each process/phenomenon. Here we broke this down into two aspects:

1. What is the state of knowledge regarding this phenomenon/process and how well has knowledge regarding this process/phenomenon been translated into measurement technologies and data analysis procedures?
2. What is the state of knowledge regarding this phenomenon/process and how well has knowledge regarding this process/phenomenon been translated into state-of-the-art modeling tools?

Conceptually, the goal of this combined rating system is to identify phenomena/processes that have high importance and where critical knowledge gaps preclude full treatment of those phenomena/processes in numerical models or current measurement technologies and data analysis tools. Such phenomena/processes will have high importance ratings but low measurement/modeling ratings. Advancing knowledge for these topics is most likely to enhance TRL for LEE solutions. In this preliminary PIRT analysis respondents were also encouraged to supply narratives explaining their rankings.

Based on PIRT tables one can identify key processes and phenomena that are of high importance but where the state-of-the-art ability to measure or simulate them is deemed good. An example is hub-height wind speeds at operating wind farms. These wind speeds are critical to power production and blade tip speed predictions. The mean ranking for phenomena importance was > 0.9 with small standard deviation (≤ 0.2) indicating consensus of this ranking. But the ratings for translation of knowledge to measurements and/or models is also rated as high. Nacelle mounted anemometers and/or remote sensing technologies such as lidars have been demonstrated to have relatively high fidelity with respect to wind speeds within the rotor plane even in complex terrain [102] and offshore [103]. Multiple modeling exercises have also demonstrated that numerical weather prediction (NWP) models such as the Weather Research and Forecasting (WRF) model, particularly when coupled to micro-scale flow models, also exhibit relatively high fidelity [104]. This does not imply there is not a need for continuing to improve measurement and modeling capabilities but that, in the context of LEE, other research activities should be prioritized.

Equally, there are processes/phenomena where understanding is lacking but uncertainty in a process/phenomenon is not deemed to be a current primary limitation on TRL for LEE solutions. Such a process/phenomenon might be deemed tier-2 for research effort. An example drawn from Theme 1 Atmospheric drivers is non-hydrometeor stressors, which received a mean process/phenomena importance level rating of 0.55 and both measurement and modeling require improvement.

High SD of rankings also conveys information about the divergence of opinions across the experts. An example from theme 1 is the estimation of impingement efficiency as a function of hydrometeor diameter [105]. The mean rating for importance is 0.55 but the variability around that is large (SD = 0.44). Thus, there is substantial variability in the opinions regarding whether 'capture' of hydrometeors of different sizes by the blade leading edge is < 1 for hydrometeors of greatest importance to damage, and whether there is uncertainty in the D and v_c dependence of impingement efficiency.

3. Discussion of exemplar research activities designed to address critical research needs identified in the PIRT process and thus to improve TRL of LEE solutions

3.1 Phenomena/processes given Tier 1 priority within the atmospheric drivers theme

Two processes/phenomena within Theme 1 were identified as tier 1 priority: Hydrometeor size distribution (HSD) and phase. The narratives supplied within the PIRT framework and past research suggest that although these are phenomena of importance, knowledge or translation of knowledge to improved measurement/data analysis procedures or to modeling tools is insufficient. Materials stresses are demonstrably a function of the number and diameter of impinging hydrometeors. The HSD (and hydrometeor phase) is also a reciprocal function of precipitation intensity and of temporal and spatial scale [106]. For example, analyses of data from the US Southern Great Plains showed that 10% of 1-minute precipitation rates exceed 4.5 $mmhr^{-1}$, while this 90th percentile value for 10-minute precipitation rates are < 2.3 $mmhr^{-1}$ [14]. A study in Switzerland using automated hail sensors found that '75 % of local hailfalls last just a few minutes (from less than 4.4 min to less than 7.7 min, depending on a parameter to delineate the events) and that 75 % of the impacts occur in less than 3.3 min to less than 4.7 min.' [107] These findings imply not only a need for robust assessments of precipitation rate, HSD and phase but also that such data, whether from measurements or models, need to be available at high spatiotemporal resolution.

A range of technologies exist to measure the precipitation intensity (collectively referred to as rain gauges (RG)) [108] and HSD (i.e. instruments that measure hydrometeor number concentrations in size classes and are referred to as disdrometers) [14]. Some disdrometers also measure the fall velocity, phase and sphericity (which is required to compute the hydrometeor mass and kinetic energy transfer) [14]. In the case of optical (or laser) disdrometers the hydrometeor D is measured by the number of horizontal laser beams broken by the hydrometeor and the v_f is derived from the duration of time the beams are interrupted.

Assuming spherical droplets, the precipitation rate (RR in $mmhr^{-1}$) from a disdrometer is proportional to the sum of the number of size-distributed (n in diameter (D) class i=1 to j):

$$RR \propto \sum_{i=1}^{j} n_i D_i^3 \quad (3a)$$

Or more explicitly for the OTT Parsivel² disdrometer (which has 32 diameter classes):

$$RR = \frac{\pi}{6}\frac{3.6}{10^3}\frac{1}{Ft}\sum_{i=1}^{32} n_i D_i^3 \quad (3b)$$

Where F is the instrument 'field of view' and t is the duration of time during which the hydrometeor counts are made.

The implication of Equation (3a,b) is that small errors in hydrometeor diameter can yield large errors in RR. Hence, if the precipitation rate is to be derived from disdrometers accurate assessment of the hydrometer diameter is a necessary pre-requisite, but the axis ratio (the ratio of the vertical dimension of the hydrometeor to the horizontal dimension) for liquid hydrometeors is generally < 1, and scales with the horizontal dimension [95,109]. Most disdrometers report RR computed by integrating over all hydrometeor diameters and fall velocities using proprietary software which includes correction factors e.g. for the axis ratio of hydrometeors that are not fully specified.

When the accumulated depth of precipitation (or precipitation intensity) from disdrometers is compared with tipping or weighing rain gauges that measure only the mass or depth of water accumulated over a time interval, incomplete closure is achieved [110]. Thus, even if using first-order models of nominal erosion rates (such as those described above) are employed, the source of the precipitation data is a major source of uncertainty in lifetime estimates. For example, data are being collected at the Wind Energy Institute of Canada (WEICan) wind farm on Prince Edward Island Canada, using an OTT Parsivel² optical disdrometer and an unheated Campbell Scientific TE525 Tipping Bucket Rain Gauge (RG) (Figure 4a). Because the RG is unheated, in the following we select only data collected during the summer months to avoid periods with snowfall. Hourly summertime accumulated precipitation from the disdrometer is consistently lower than those from a RG across a wide range of precipitation rates and wind regimes (Figure 4b,c). Although the disdrometer is more likely to report non-zero precipitation (even when the threshold to detect precipitation is set to that determined by the tip-volume of the rain gauge, Figure 4d), of particular importance to LEE, the RG at WEICan exhibits twice the frequency of occurrence of precipitation rates > 10 mm/hr. When conditionally sampled to select periods when both sensors exhibited non-zero precipitation, the probability of extreme precipitation being reported by the RG is also higher than that from the disdrometer (Figure 4c).

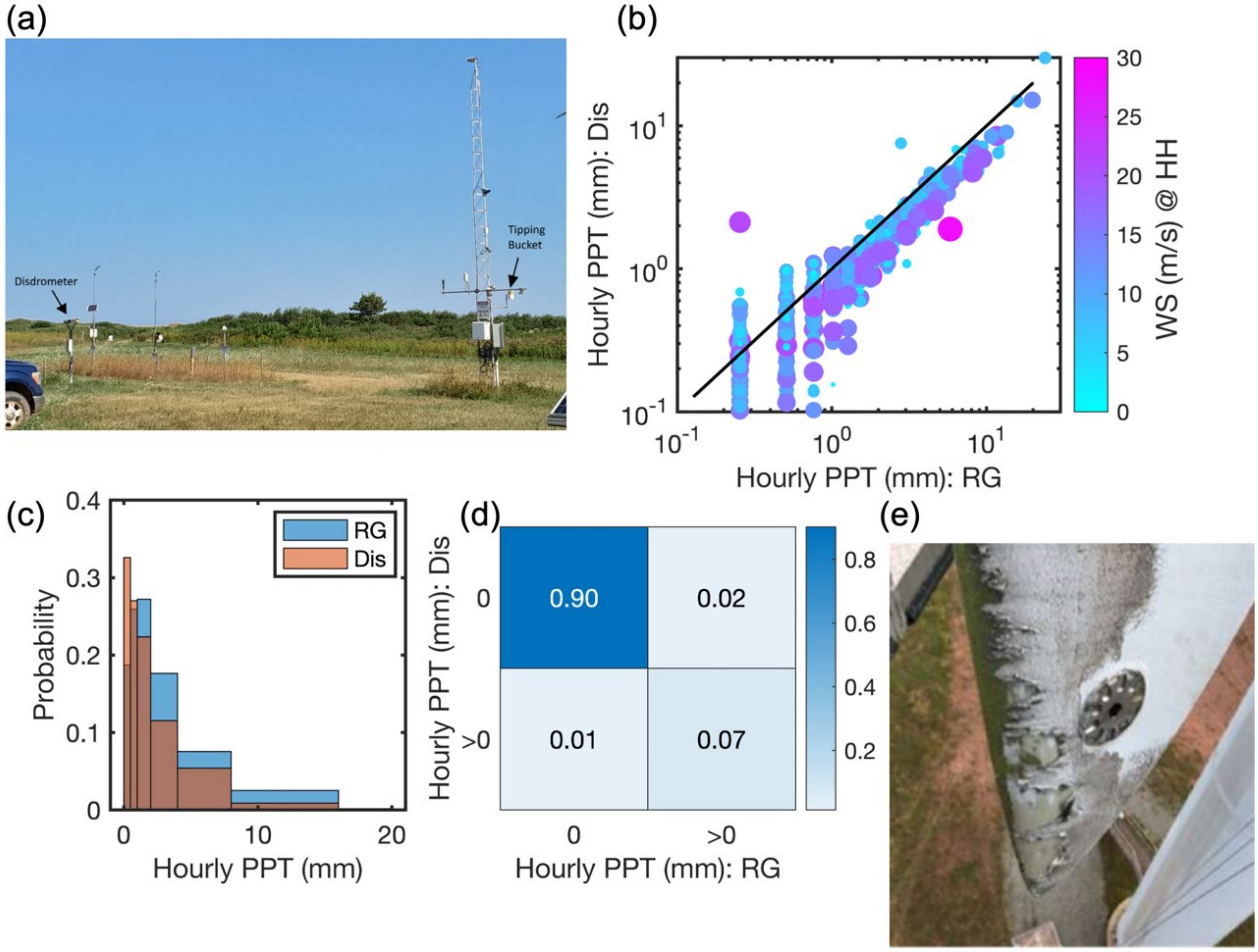

Figure 4 (a) Precipitation sensors deployed at WEICan. (b) Scatterplot of hourly precipitation (PPT) from the rain gauge (RG) and OTT disdrometer (Dis) for data collected during; May-October of 2002 and 2023. Symbols scale with prevailing wind speed at wind turbine hub-height (HH). (c) Histograms of hourly precipitation for all hours when both sensors report non-zero precipitation. (d) Heatmap of the joint probability of no precipitation (defined using a threshold of 0.126 mm, i.e. minimum reported by the RG) from RG and Dis. As shown, 7% of hours exhibited precipitation of > 0.126 mm from both sensors. (e) Example photograph of leading edge erosion on one of the wind turbines operating at WEICan.

More mechanistic models of material stress and erosion include information regarding HSD (i.e. the number concentration of hydrometeors of given diameters, D_i) which can be derived from disdrometer measurements of the number counts ($n(i,v)$) in diameter (i) and fall velocity (v_f) classes:

$$N(D_i) = \sum_{v=1}^{x} \frac{n(i,v)}{Ftv_f(\mathrm{i},v)\Delta D_i} \quad (4)$$

Where x is the number of fall velocity classes and ΔD_i is the width of each diameter class, i. The implication of Equation (4) is that small errors in either hydrometer D or fall velocity can yield substantial errors in the derived HSD (i.e. expression of number concentrations as a function of hydrometeor diameter). However, measured HSD also differ across different disdrometers and standardized data processing procedures are lacking [14,95,111]. Further, there is evidence that the relative performance of different disdrometers is a function of the prevailing climate [14]. Accordingly, when measurements from the three most commonly used disdrometers types (optical, impact and video) are used to compute accumulated kinetic energy of transfer from hydrometeor impacts to wind turbine blades at an example site in the US Southern Great Plains, the results differ by 38% [95]. The results differ by 100% when different data analysis protocols that vary in terms of the permitted range of fall velocities regarding hydrometeor asymmetry are applied to a single disdrometer [95]. Also, even excluding effects from hydrometeor hardness, hail may be substantially more erosive than rain due to the higher diameters of these hydrometeors. Many disdrometers use proprietary empirical functions to indicate possible presence of hail based on hydrometeor diameter and/or fall velocity rather than directly detecting it.

Research to reduce uncertainty in HSD/v_f/sphericity (axis ratio)/phase and ultimately to provide best practice for measurements at prospective or operating wind farms is ongoing. This includes an experiment performed at an airport in upstate New York in which two identical OTT Parsivel² optical disdrometers have been deployed close to a highly maintained Mesotech heated tipping bucket RG (part number 29000503) deployed as part of the Automated Weather Observing System operated by the US Federal Aviation Administration. The experiment ran from June to September 2024, inclusive (154 days of 1-minute observations), and focused on summer months to avoid snowfall periods. It is designed to test whether the presence of large diameter hydrometeors reported at $v_f < v_t$ (where v_t is the terminal fall velocity) for that D [112] is due to horizontal advection of the droplets during high wind events. Accordingly, one of the disdrometers was deployed with a windshield and the other without as typifies current deployments at operating wind farms (Figure 5a). In contrast to the data being collected at WEICan (Figure 4) good achievement is found between hourly precipitation intensity from the RG and disdrometers across the entire dynamic range of the precipitation intensities (Figure 5b). Across the range of observed wind speeds (0-12 ms^{-1}) and wind gusts (0-18 ms^{-1}) measured using a sonic anemometer deployed at 10-m AGL, the two disdrometers exhibit a high degree of agreement in terms of detection of precipitation (Figure 5d) and amount of precipitation (Figure 5b), and there is no evidence that the degree of agreement between the disdrometers and with the RG scales with wind intensity (Figure 5b). This experiment does not suggest that wind shielding of disdrometers greatly reduces the frequency of occurrence of hydrometeors falling with $v_f < v_t$ (Figure 5c), or greatly improves agreement with precipitation rates sampled with a RG (Figure 5b).

There remains an urgent need for a comprehensive instrument inter-comparison experiment, openness from instrument manufacturers regarding hardware settings and for development of best practice for instrument deployment and data processing to enhance the TRL for prediction of long-term LEE and nowcasting of erosive events for erosion-safe mode implementation.

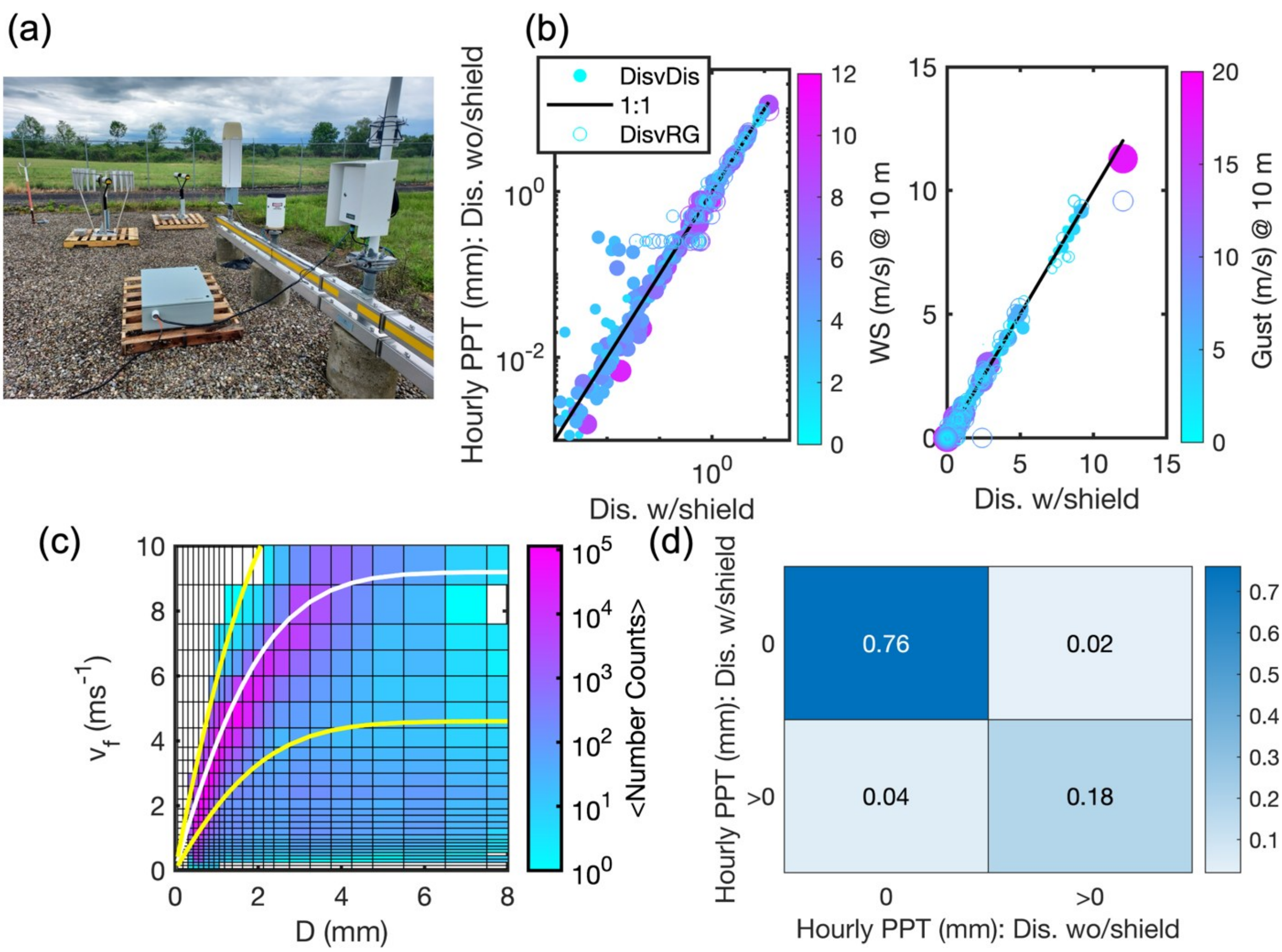

Figure 5. (a) Instruments deployed in upstate New York. (b) Scatterplot of hourly precipitation (PPT) from the disdrometer operated without the wind shield (Dis wo/shield) versus the disdrometer with the wind shield (Dis w/shield) (filled symbols) and the rain gauge (RG) (open symbols) on logarithmic and linear axes. Symbols are scaled with, and colored by, the prevailing wind speed at 10 m AGL (left-hand panel) and by the fastest wind gust (right panel). (c) Joint probability of hydrometeor diameter (D) and fall velocity (v_f) from Dis w/shield. White line indicates terminal fall velocity (v_t) as a function of D from Gunn and Kinser [112]. Yellow lines show the ±50% bounds on v_t that may indicate erroneous observations [113]. (d) Heatmap of the joint probability of no precipitation or precipitation from the two disdrometers.

NWP models are sophisticated and skillful tools for weather forecasting and climate projections. However, simulated precipitation occurrence and intensity remain less skillful than other atmospheric properties and are highly dependent on model grid [114]. The PIRT analysis also identified the need for improvements in the numerical simulation of precipitation and HSD. These issues have long been recognized within the atmospheric science modeling community [115] and there are many parameterizations available to represent cloud, precipitation, and convection processes from scales of millimeters to kilometers, which can yield very different precipitation rates (see example in Figure 6). Most NWP models use bulk microphysics schemes and employ gamma distributions for cloud and hydrometeor distributions [116-120]. Binned (or classed) microphysics schemes resolve the HSD at higher computational cost and improved flexibility [121], but different schemes yield widely varying hydrometeor characteristics [122] and they do not always out-perform bulk schemes in terms of the fidelity of RR [123]. Most modeling studies post-process simulated RR using empirical relationships between near-surface HSD and simulated RR [124]. Simulated hail production is also very sensitive to the pre-existing aerosol, frozen hydrometer density and other factors influencing hydrometer diameters and fall velocities [125]. The land surface scheme employed and soil moisture used to initialize numerical simulations also influence precipitation simulation fidelity [126].

It has been previously shown that WRF exhibits some skill for forecasting heavy precipitation and hail and the occurrence of high wind speeds, but the joint occurrence of heavy precipitation and high wind speeds and the simulation of hail diameter continue to lack the fidelity necessary to make integrative robust assessments of erosion potential or short-term forecasts of highly erosive events for erosion safe-mode operation [75, 76].

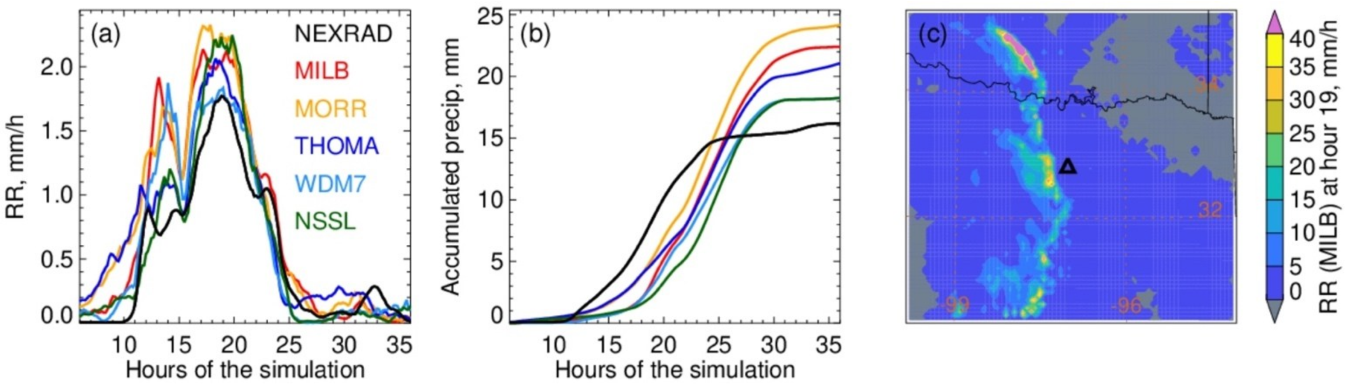

Figure 6 Spatial average; (a) Precipitation rate and (b) accumulated precipitation from WRF simulations (dx = 1 km) of an intense precipitation event during March 2017 over a region with many wind turbine assets [127]. The simulation [128] is performed in a short-term forecasting mode as would be used for predicting the need for erosion safe-mode operation of wind turbines. Time series denote simulations with five different microphysics schemes; Milbrandt-Yau (MILB), Morrison (MORR), Thompson aerosol aware (THOMA), WRF double moment seven category (WDM7), and NSSL, plus RADAR (NEXRAD) observations. (c) The domain over which the spatial averaging is performed. Black triangle indicates Dallas Fort Worth, black lines denote the state boundaries of Texas, Oklahoma and Arkansas.

Improved representation of hydroclimatic conditions with numerical models, scoping of uncertainty and fundamental model improvements are a focus of multiple initiatives within the atmospheric science community including the World Climate Research Programme Global Precipitation Experiment lighthouse activity [129]. Machine learning climate emulators are also being developed that seek to bridge the gap between the scales resolved by NWP models and precipitation at the local-level [130]. Leveraging such initiatives can, and will, benefit the wind energy industry and enhance TRL of LEE mitigation options. However, the specific need for model and measurement fidelity for precipitation rates and HSD particularly at high wind speeds is, to some degree, specific to the wind energy community. Effort should be invested in a detailed NWP verification and validation (V&V) framework that is specifically focused on the requirements of the wind energy community to advance the TRL for model-based prediction of LEE meteorological drivers. This is a focus of the Understanding atmospheric impacts on wind turbines for better efficiency (AIRE) project (https://aire-project.eu).

3.2 Phenomena/processes given Tier 1 priority within the damage detection and quantification theme

This PIRT process resulted in one phenomenon/process being given Tier 1 priority within the damage detection and quantification theme: Translating water impingement to materials loss/stress (e.g. metrics: Kinetic Energy, Springer-ADF, VN curves). Although this topic could legitimately be included under theme 3 – materials response, the specific theme under which it was listed is likely not a critical determinant of the PIRT rating. As described above, computing the accumulated kinetic energy (AKE) of collisions between falling hydrometeors and rotating blades through time is trivial presuming adequate data regarding the hydrometeors and hub-height wind speed are available at high time resolution. However, AKE does not directly translate to material damage.

Springer's model uses material properties of the blade and coating and the hydrometeor impact number, diameter, velocity and impact angle to estimate a distance to failure or the end of the incubation period for coating wear for each hydrometeor diameter that combined with Miner's rule is used to estimate ADF [95]. However, Springer's model is not very mechanistically defined and the parameter estimates are highly uncertain [66].

As described above many RET experiments are confined to a fairly narrow range of droplet sizes and can generate only liquid droplets. However, actual precipitation is comprised of an ensemble of multiple hydrometeor diameters. A recommended practice from DNV [131] considers only one droplet diameter (D = 2.38 mm) that naturally will not reflect the range of observed hydrometeors. Indeed, based on data from the US Southern Great Plains, where deep convection and intense precipitation is relatively common [14], the mass-weight hydrometeor mean diameter is ≥ 2.38 mm during only 6% of 1-minute precipitation periods. Further, to achieve damage results in a reasonable time (i.e. to accelerate erosion), RETs are operated at higher closing velocities than represent real operating conditions. The resulting VN-curves are then extrapolated to derive estimates at lower v_c of the number of impacts at a given diameter that would yield damage. Testing viscoelastic coatings at very high closing velocities may result in rain erosion testers underestimating coating or LEP durability because wind turbines frequently operate at lower tip-speeds. A comprehensive rain erosion test with multiple droplet sizes underlines the need for further research on the derivation of the VN-curves from RETs [132]. More detail is given in section 3.3.

Other phenomena/processes in the damage detection theme that are characterized as tier 2 priority for research relate to the accuracy of damage estimates. The use of drones and robots for blade inspection is becoming more routine particularly for larger wind turbines and offshore wind farms and potentially decreases costs/time/risk of injury to technicians [133]. Full automation of damage detection data derived using such tools is leveraging advanced Machine Learning (ML) image processing tools [62,134]. Further innovations in this field include construction of digital twins using high-resolution topographic leading edge roughness (LER) data from operating/decommissioned blades that can be analyzed aerodynamically using 3-D computational fluid dynamics (CFD) or wind tunnels [135].

Efforts to commercialize damage detection solutions are ongoing (e.g. using thermal imaging [136], laser profilometry [137] or gloss measurement [138]) implying relative high TRL, even as research is being conducted to evaluate efficacy as a function of damage severity and extent [139].

3.3 Phenomena/processes given Tier 1 priority within the materials response theme

This PIRT analysis identified two phenomena within Theme 3: Materials response as Tier 1 priority for research that links to the usefulness of RETs and specifically their representation of atmospheric conditions including hydrometeors phase (e.g. rain and hail), size distributions & collision velocities [12], and whether accelerated lab-tests represent pre-stressing of blade materials that enhances hydrometeor erosion of the leading edge [140]. These concerns also link to the second Tier-1 research priority: Methodologies to translate lab experimental data (incl. rain erosion testers) to field conditions & failure modes (see section 3.2).

Important new research is testing multiple key aspects of translation of RET to real-world conditions. For example, RET tend to operate with continuous bombardment with droplets, while in the real-world precipitation is discontinuous. Experiments with a pulsating jet erosion tester has evolved evidence that duration of time between precipitation events may play a role in the dictating the number of droplet impacts required to reach the end of the incubation time [141]. Recent RET tests performed with and without UV exposure have found that UV weathering reduced the LEE coating life by about 30%, which greatly influenced resulting VN curve parameters [142].

Experimental technologies clearly have an important role in projecting damage emergence and progression, but mechanistically-sound numerical models can permit more diagnostic analyses and sampling across a broader spectrum of conditions. An important source of uncertainty in such numerical models is that the precise composition of LEPs and/or coating is proprietary. In addition, the temperature and strain rate sensitivity of the flow stress are either ignored in modeling or at best implemented with empirical constitutive equations. This may lead to significant deviations from reality considering the adiabatic nature of hydrometeor impacts deforming surface layers at relatively high strain rates [143].

More sophisticated and explicit models such as Finite Element (FE) models of multiple liquid impact on multilayered viscoelastic materials take into account microscale materials structure and porosity [84,144] and thus are preferable to empirical or semi-empirical models. However, they are relatively computationally demanding and require information regarding a range of material properties and behaviors that can be difficult to acquire. The computational cost is amplified if all possible combinations of hydrometeor diameter and closing velocity are to be included in coating lifetime estimations. Thus, an emerging area of research is construction of ML emulators conditioned using output from numerically sophisticated models but taking the form of considerably faster closed-form architectures [145]. Such emulators can be used to more rapidly and efficiently evaluate uncertainty space. An example is the incorporation of a ML model trained by the output of FE simulations of the spatial and temporal evolution of the stress field in the coating for various impact speeds and hydrometeor diameters (see schematic in Figure 7). To illustrate this potential a surrogate model based on a neural network was trained to make predictions for the peak stresses in the coating layer. A relatively small number of FE simulations was used to generate training data for droplet diameters (D) of 0.5 to 4 mm and impact speeds (v_c) between 80 and 90 ms^{-1}. A neural network surrogate model was trained to predict peak von Mises stresses at each point in the coating as a function of D and v_c. An independent set of FE simulations was used to evaluate the surrogate model predictions (Figure 8). The ML predictions capture the topology of the peak stress contour, but the peak values show an error ~ 10% relative to independent FE simulations. Building a larger suite of training simulations would likely aid in building a more robust surrogate model.

In principle, the workflow shown in Figure 7 could be expanded such that wind speed, rain intensity and HSDs measured or modeled for any location can be combined with the surrogate model to obtain coating stresses for all possible combinations of impact parameters in an analogous manner to their use with the Springer model. The properties of the coating material could also be used as input to the machine learning model, and in principle this workflow can be extended to estimate not only to lifetimes of coatings, but also to levels of surface damage for estimating AEP losses.

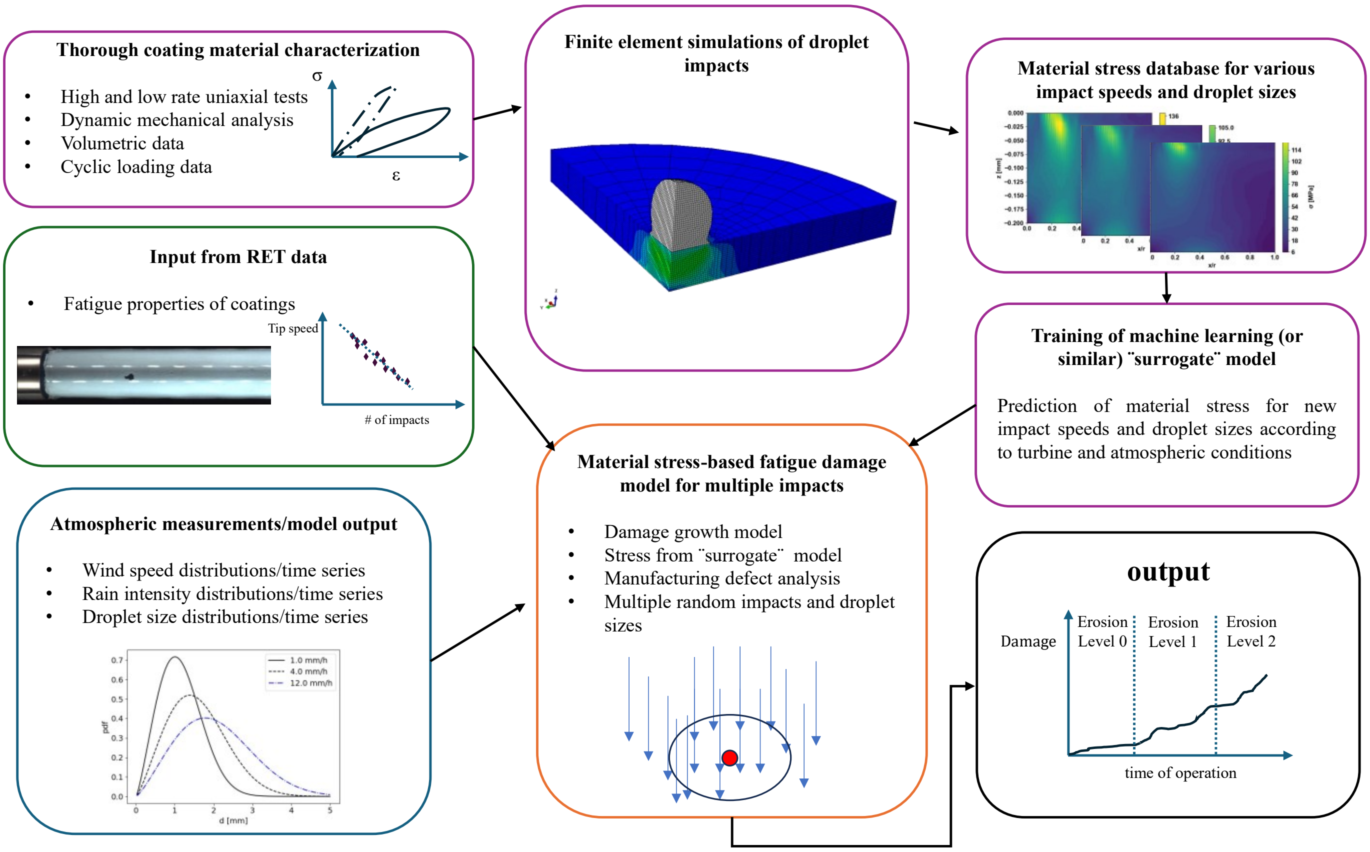

Figure 7 Schematic of a proposed combination of material testing and modeling, atmospheric measurements and lifetime modeling through the use of a machine learning surrogate model.

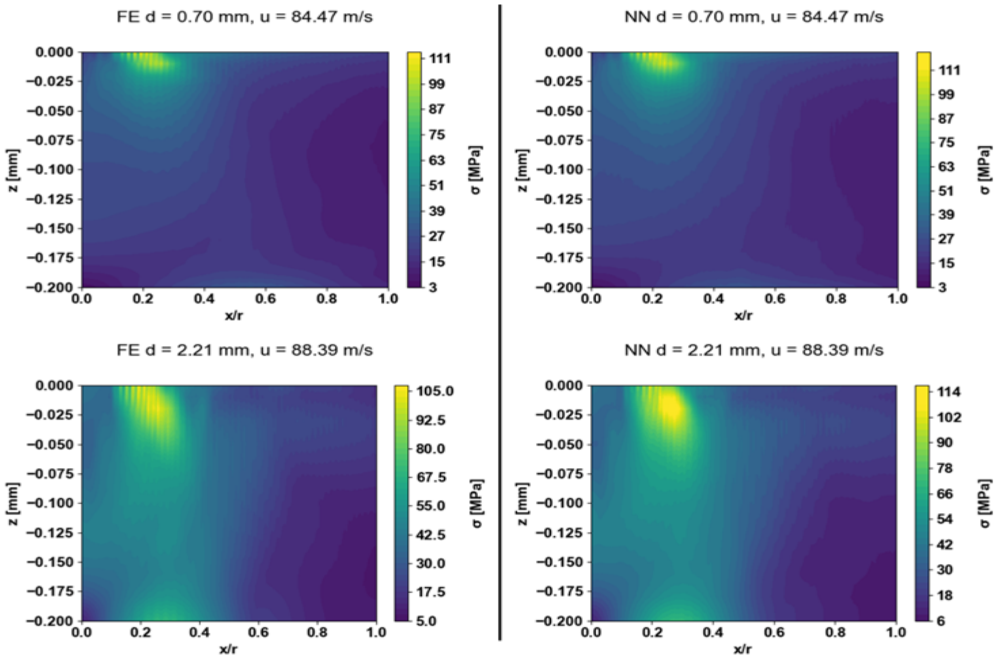

Figure 8 Comparison of peak von Mises stress (σ in MPa) contours over a cross section of the coating layer that spans from the top surface (z=0) to the full layer thickness (z=0.2 mm) and from the impact axis (x/r=0) to a distance equal to the droplet radius r (x/r=1) based on the finite element (FE) simulations (left) and the predictions of the neural network surrogate model (NN) (right) for two different hydrometeor diameters (d) and closing velocities (u).

While use of ML-based surrogate models shows great promise, the response of viscoelastic polyurethane-based coatings depends on the loading rate, temperature and the level of experienced strain. A more thorough experimental characterization of these materials is required, which includes high and low-rate uniaxial data for wide strain ranges, dynamic mechanical analysis, cyclic loading-reloading and volumetric strain measurements. Data from RET experiments can aid in determining parameters related to the fatigue behavior of coatings and to enhance the accuracy of predictions. Improvements in experimental procedures related to RET are therefore also highly valuable.

3.4 Phenomena/processes given Tier 1 priority within the aerodynamics theme

Finally, three phenomena/processes were identified as Tier 1 priority in the aerodynamic implications theme: (a) Quantification of damage and surface roughness progression through time. This links strongly to theme 2 – damage detection. (b) Attribution of AEP loss to LEE (via effective surface roughness). (c) Optimization of damage repair solution/timing.

Quantification of wind turbine power and AEP losses due to LEE typically relies on blade force coefficient data obtained with wind tunnel testing or simulations with computational fluid dynamics (CFD) models [146,147]. In both cases, the geometry of damage and corresponding surface roughness at any time between installation and leading edge resurfacing are key to achieving reliable estimates of the blade performance degradation. For moderate to intermediate LEE, which typically corresponds to damage of the thin external protection system of the leading edge (e.g. coating), the effects of roughness can be modeled by means of the equivalent sand grain roughness [148]. The equivalent roughness height, yielding the same wall shear stress as that achieved with the observed roughness, can be obtained by using geometry-, experimental data or very high-fidelity CFD [149]. Their use for LEE applications, however, is associated with uncertainty, in part due to the difficulty of measuring blade roughness with sufficient resolution. One of the aims of the Leading Edge Roughness categorization (LERcat) efforts is to reduce this uncertainty [76]. When LEE becomes severe, with damage also to the leading edge composite material, the sand grain model is no longer applicable, and the erosion geometry needs to be resolved [150]. The above highlights the importance of acquiring, with sufficient resolution, the depth and surface map of LEE and thus links to new innovations in damage characterization mentioned under Theme 2.

Once erosion topographies are acquired with adequate geometric resolution, ML can also play a key role in developing blade predictive maintenance frameworks by providing erosion aerodynamics and resulting AEP losses, as demonstrated with the AEP loss prediction system (ALPS) [146]. Determining the LEE-induced blade performance degradation for each erosion topography encountered in operation would require numerous lengthy CFD analyses and specialized expertise for each wind turbine assessment, a cost increased by the large number of turbines in a wind farm and the potentially high temporal frequency of these assessments in the wind farm lifetime. An initial (one-off) execution of many CFD simulations corresponding to many diverse erosion topographies can be used to train the fast ML metamodels that be used to quickly determine blade force coefficients for AEP loss assessment. Preliminary work, shown in Figure 9 [146], has demonstrated the high reliability of fast ML metamodels for predicting lift coefficient (c_l) and drag coefficient (c_d) of eroded blade sections, allowing the ML models to be used for AEP loss assessment [150,151]. More development work is needed in this area to; generalize these ML approaches, enable them to consider even wider LEE patterns observed in operation, and consider the variability of the nominal blade geometry among different wind turbine classes.

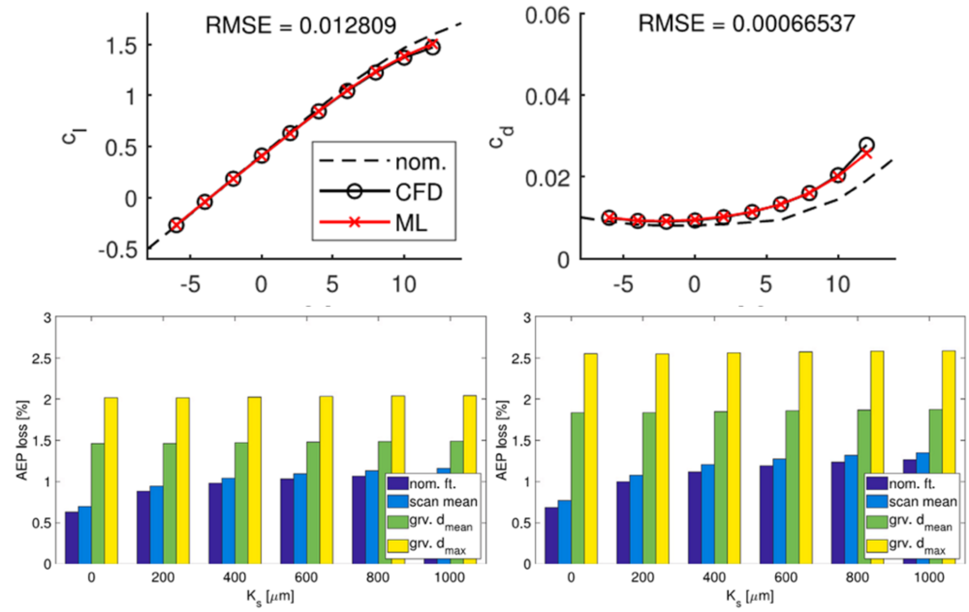

Figure 9 Top: Eroded blade section force coefficients (lift (C_l) and drag (C_d)) for varying angles of attack (bottom axis) from geometry-resolving CFD ('CFD') and ML models ('ML') trained using metadata of the erosion topography (curve labelled 'nom.' denotes nominal section performance curves) [128]. Bottom: offshore (left) and onshore (right) AEP losses for a multi-MW wind turbine derived using blade section force coefficients from ML models of type displayed in top plots for broad patterns and extent of erosion topographies; 'Ks' = equivalent sand grain roughness, 'nom/ ft.' & 'scan mean' denote moderate to intermediate LEE severity, and 'grv. d_{mean}' & 'grv. d_{max}' denote severe LEE stages [150].

Optimizing the timing of blade leading edge repair was identified as an important phenomena/process in the PIRT. Optimization of repair at any operating wind farm depends on factors such as wind turbine age, damage severity, cost of electricity and accessibility. Considerations used by commercial wind farm owner/operators regarding repair decisions are usually considered proprietary and thus are held in confidence. Thus, information from WEICan is briefly presented below to illustrate the process by which repair decisions and LEP application were made and the results of those actions. WEICan owns and operates five 2 MW turbines on a coastal, high wind site with turbines 1-4 being locations on an escarpment and experiencing a very similar wind climate [152]. All wind turbines at WEICan have exhibited advanced levels of LEE since commissioning in 2013. WEICan have chosen to initiate repair measures prior to "moderate" or "severe" levels of erosion, and indeed before there was significant mass loss or clear detection via power curve degradation or acoustic tracking [153], due to factors such as the severity of the winter climate that means the O&M window is relatively short and the remote location that means access for more extensive O&M is challenging. The two main indications that trigger WEICan's decision to carry out a blade repair are:

1. Rapid degradation of LEP. If a LEP product experiences significant peeling and bubbling within a year, it saves on repair expenses to replace it before the blade is completely exposed.
2. First sign of visible fiberglass. The more fiberglass is eroded away, the more blade preparation work is required before repairs. With light erosion, only sanding and buffing of the surface is required before reapplying the LEP, which takes about half a day per blade. With moderate to heavy erosion, the blade must be sanded, built back into shape with additional fillers and fiberglass before reapplying the LEP product,

which can take 1.5 days to 2 days per blade. Therefore, repairing blades at the first sign of visible fiberglass saves time and cost.

Initially, the blades on the wind turbines deployed at WEICan had no LEP, only standard polyurethane paint. In 2014, after LEE was observed visually, the blades were repaired, and standard polyurethane paint was re-applied. LEE was observed again in 2015. Since 2016, WEICan has engaged in testing of five different LEPs, including paints, tapes, and shells. The first four LEPs were applied from 30 m to 45 m, while the fifth LEP was applied from 35 m to 45 m, measuring from the root of the blade. Each type of LEP has specific application instructions which typically require filling, sanding, and cleaning to achieve a smooth surface; and specify maximum and minimum temperatures and relative humidities for curing and drying. Most of the wind turbine blade LEP materials have failed in one year to two years (Table 2, see example in Figure 4e), which LEP manufacturers generally have attributed to improper or inadequate surface preparation and installation. For example, epoxies or adhesives were not appropriately activated, surface was not adequately cleaned, blade repairs with fillers or coatings ahead of installation were still curing, conditions may have been appropriate at the start but were not sustained, or the skills of technicians was not adequate. The original blade quality has also been identified as an important factor impacting LEP failure.

Table 2. Leading edge protections used, dates applied and damage and failures observed at WEICan.

Type of LEP	Turbine	Year Applied, Year Reapplied	Year Damage Observed	Types of Damage Observed
Paint (2 component epoxy)	T1, T5	2016, 2017, 2019	2017, 2019, 2021	Pitting, cracking, peeling, bubbling
Paint (polyurethane)	T4	2016, 2017, 2019	2017, 2019, 2021	Pitting, peeling
Tape (2-component polyurethane)	T2	2016, 2017	2017, 2021	Pitting, peeling, bubbling
Tape (2-component polyurethane)	T3	2016, 2019	2019, 2021	Pitting, peeling, bubbling
Shell (polyurethane)	T1	2021, 2023	2023	Peeling, bubbling
	T2	2022		
	T3	2022		
	T4	2021, 2022	2022	Peeling, bubbling
	T5	2022		

Current leading edge repair work instructions have many requirements, including filling, sanding, and cleaning with maximum and minimum temperatures and relative humidities for curing and drying, as well as wind speed restrictions, depending on the method used to access the blade. This leads to small windows of time where repair is even possible and long and expensive repair times. TRL would be enhanced by simplifying the repair process so that there are fewer restrictions, and it can be done more quickly and economically.

A Tier 2 priority in theme 4 relates to the aerodynamic performance reductions due to LEP and their efficacy in slowing LEE. Data from the WEICan wind turbines was used in a decomposition analysis to remove effects due to prevailing meteorology (e.g. changes in the wind speed distribution before and after application) and isolate the impact of LEP on wind turbine performance. The results showed minimal to no improvements in performance due to LEP application and resulting smoothing of the blade [153]. This is likely due to the high proportion of time WEICan's wind turbines spend operating at rated power when AEP loss due to LEE is minimum, as well as the fact that WEICan repairs blades before any reduction in performance is observed.

Ultimately, decision-making with regards to LEE at WEICan relies on information from many of the Tier I and Tier II themes: existing and expected progression of damage, the resulting AEP reductions, and impacts of LEP options. Uncertain durability of LEP options, perhaps resulting from unreliable LEP installation, has been the most substantial barrier to effective O&M planning for this site.

4. Concluding Remarks and Next Steps

The PIRT tables presented herein represent the first attempt to collate expert judgements on research priorities to enhance the TRL for solutions to reduce AEP (and revenue) losses and wind turbine operation and maintenance costs caused by wind turbine blade LEE. We used a snowball sampling technique to identify possible respondents [81] and had a relatively small sample size (n < 20). Thus, the results must be considered preliminary. Nevertheless, the PIRT presented herein yields some important insights and lays the foundation for a comprehensive PIRT survey of wind energy experts that will be conducted during 2025 via the International Energy Agency Wind Energy (IEA) Technology Collaboration Programme (TCP) Task 46: Leading Edge Erosion.

PIRT analyses are valuable because they allow systematic identification of phenomena/processes of importance and that require further research to enhance TRL or reduce safety risks. However, PIRT analyses are inherently subjective, since they leverage expert knowledge and judgment [82]. While some have advocated that PIRT methodologies should be based on literature-based meta-analyses [83], these too are not fully objective due to inherent biases in publishing [84]. An important advancement of this PIRT analysis is that the standard deviation of rankings across respondents is captured and presented to provide quantitative information about the presence or absence of consensus in the rankings. Divergence of opinion may derive from knowledge gaps due to the trans-disciplinary nature of a topic or the rapidly evolving nature of a complex topic. Expert-knowledge based frameworks for research priority identification using PIRT may also not fully reflect emerging issues. An example of this that was identified in the PIRT but not given a Tier 1 ranking is possibility of micro-plastic shedding to the ocean environments. This research topic is being addressed in the Preventing MIcroplastics pollution in SEa water from offshore wind (PREMISE) project [154]. Emergence of such new topics strongly advocates for PIRT assessments to be continuously updated to ensure they evolve as knowledge is advanced.

The PIRT process and discussions summarized above indicate the TRL for LEE solutions remains relatively low. However, investment in the priority areas articulated herein will enhance fundamental understanding and can be used to evolve robust framework for end-to-end LEE prediction (Figure 7). Investments should be made in building a robust model V&V framework for each component of such a model chain [155]. Successful implementation of such a framework will require sharing of a range of data from industrial partners. Needed information include LEP product material properties, greater transparency regarding hardware settings in meteorological sensors and data from operating wind farms linking LEE state and AEP. End-to-end assessment of damage as a function of operating climate would also greatly benefit from sharing of blade damage reports/images from operating wind farms for use in evaluation of location specific meteorologically-driven LEE predictions [34]. Availability of time-histories of wind turbine Supervisory Control and Data Acquisition (SCADA) data and adequately resolved LEE topographies for eroded blades will enable faster progress in blade predictive maintenance technologies.

Nomenclature

ADF Accumulated Distance to Failure

AEP Annual Energy (electricity) Production
AKE Accumulated Kinetic Energy
CAPEX CAPital EXpenditures
CFD Computational Fluid Dynamics
D Hydrometeor Diameter
Dis Disdrometer
FE Finite Element
HSD Hydrometeor Size Distribution
IEA International Energy Agency
LCoE Levelized Cost of Energy
LEE Leading Edge Erosion
LEP Leading Edge Protection
LER Leading Edge Roughness
LERcat Leading Edge Roughness categorization
ML Machine Learning
NWP Numerical Weather Prediction
O&M Operations and Maintenance
PIRT Phenomena Identification and Ranking Tables
PPT Precipitation
RET Rain Erosion Tester
RG Rain Gauge
RR Precipitation (or Rain) Rate
SALT Simplified Aerodynamic Loss Tool
SCADA Supervisory Control and Data Acquisition
SD Standard Deviation
TRL Technology Readiness Level
UAV Unmanned Aerial Vehicle
USA United States of America
UV-A Ultra Violet radiation at wavelengths (λ) = 320 and 400 nm
VN curves Velocity-Number of impacts to failure
V&V Verification and Validation
WARERs Whirling-Arm Rain ERosion testers
WRF Weather Research and Forecasting
v_c Closing velocity
v_f Fall velocity
v_t Terminal fall velocity

Author Contributions: Conceptualization, SCP and RJB.; methodology, SCP and RJB; software, SCP; validation, SCP and RJB; formal analysis, SCP, RJB, MR, HN, SC and AT; investigation, all authors; resources, SCP; data curation, SCP, AT, MR and HN; writing—original draft preparation, SCP and RJB; writing—review and editing, all authors; visualization, SCP, RJB, MR, HN, AT, SC; supervision, SCP; project administration, SCP, RJB; funding acquisition, SCP, RJB, CBH and BM. All authors have read and agreed to the published version of the manuscript.

Funding: This research was funded by the US National Science Foundation (2329911 to SCP and RJB), Sandia National Laboratory (to SCP) IEA task 46 "Erosion of wind turbine blades", EUDP grant J.nr. 64021-0003 (to CBH) the HORIZON Europe Grant "AIRE" (101083716) (to CBH and BM) and by Danish-American Innovation Network for Wind Energy (DAINWE, grant no. 2084-00014B) funded by the Danish Agency for Higher Education and Science. Computational resources to SCP and RJB used in these analyses are provided by the NSF Extreme Science and Engineering Discovery Environment (XSEDE2) (award TG-ATM170024).

Data Availability Statement: The PIRT results are summarized in Table 1. All other data can be provided upon request to the authors.

Acknowledgments: The authors acknowledge the PIRT analysis respondents and the contributions of Joachim Reuder and Mostafa Hassani to development of the PIRT. The Cornell University team gratefully acknowledge Jeffry Reimel (FAA) and Roxan Noble (Director) for enabling access to the Ithaca Airport AWOS site and Fred Letson for his assistance with instrument maintenance. WEICan gratefully acknowledge research support from Robbie Sanderson.

Conflicts of Interest: The authors declare no conflict of interest.

References

1. Pryor, S.C.; Barthelmie, R.J.; Bukovsky, M.S.; Leung, L.R.; Sakaguchi, K. Climate change impacts on wind power generation. *Nature Reviews Earth & Environment* **2020**, *1*, 627-643, doi:10.1038/s43017-020-0101-7.
2. Barthelmie, R.J.; Pryor, S.C. Climate Change Mitigation Potential of Wind Energy. *Climate* **2021**, *9*, 136, doi: 110.3390/cli9090136.
3. Gökgöz, F.; Güvercin, M.T. Energy security and renewable energy efficiency in EU. *Renewable and Sustainable Energy Reviews* **2018**, *96*, 226-239.
4. Borba, P.C.S.; Júnior, W.C.S.; Shadman, M.; Pfenninger, S. Enhancing drought resilience and energy security through complementing hydro by offshore wind power—The case of Brazil. *Energy Conversion and Management* **2023**, *277*, 116616.
5. GWEC. *Global wind report 2024*; Global Wind Energy Council, Brussels, Belgium. Available for download from:https://gwec.net/global-wind-report-2024/: 2024; p. 168.
6. Lazard. *Lazard's Levelized Cost of Energy Analysis—Version 16.0 [Online]*; Available for download from: https://www.lazard.com/research-insights/levelized-cost-of-energyplus/: Zurich, Switzerland, 2023.
7. Bolinger, M.; Wiser, R.; O'Shaughnessy, E. Levelized cost-based learning analysis of utility-scale wind and solar in the United States. *Iscience* **2022**, *25*, 104378.
8. Barthelmie, R.J.; Larsen, G.C.; Pryor, S.C. Modeling Annual Electricity Production and Levelized Cost of Energy from the US East Coast Offshore Wind Energy Lease Areas. *Energies* **2023**, *16*, 4550.
9. Rinaldi, G.; Thies, P.R.; Johanning, L. Current status and future trends in the operation and maintenance of offshore wind turbines: A review. *Energies* **2021**, *14*, 2484.
10. Du, Y.; Zhou, S.; Jing, X.; Peng, Y.; Wu, H.; Kwok, N. Damage detection techniques for wind turbine blades: A review. *Mechanical Systems and Signal Processing* **2020**, *141*, 106445.
11. Bech, J.I.; Hasager, C.B.; Bak, C. Extending the life of wind turbine blade leading edges by reducing the tip speed during extreme precipitation events. *Wind Energy Science* **2018**, *3*, 729-748.
12. Bartolomé, L.; Teuwen, J. Prospective challenges in the experimentation of the rain erosion on the leading edge of wind turbine blades. *Wind Energy* **2019**, *22*, 140-151.
13. Zhang, S.; Dam-Johansen, K.; Nørkjær, S.; Bernad Jr, P.L.; Kiil, S. Erosion of wind turbine blade coatings–design and analysis of jet-based laboratory equipment for performance evaluation. *Progress in Organic Coatings* **2015**, *78*, 103-115.
14. Pryor, S.C.; Barthelmie, R.J.; Cadence, J.; Dellwik, E.; Hasager, C.B.; Kral, S.T.; Reuder, J.; Rodgers, M.; Veraart, M. Atmospheric Drivers of Wind Turbine Blade Leading Edge Erosion: Review and Recommendations for Future Research. *Energies* **2022**, *15*, 8553, doi: 8510.3390/en15228553.
15. Sareen, A.; Sapre, C.A.; Selig, M.S. Effects of leading edge erosion on wind turbine blade performance. *Wind Energy* **2014**, *17*, 1531-1542.
16. Mishnaevsky Jr, L.; Hasager, C.B.; Bak, C.; Tilg, A.-M.; Bech, J.I.; Rad, S.D.; Fæster, S. Leading edge erosion of wind turbine blades: Understanding, prevention and protection. *Renewable Energy* **2021**, *169*, 953-969.
17. Gaudern, N. A practical study of the aerodynamic impact of wind turbine blade leading edge erosion. *Journal of Physics: Conference Series* **2014**, *524*, 012031, doi:10.1088/1742-6596/524/1/012031.
18. Froese, M. Wind-farm owners can now detect leading-edge erosion from data alone. *Windpower Engineering and Development* **2018**, *August 14, 2018*.
19. Campobasso, M.S.; Castorrini, A.; Ortolani, A.; Minisci, E. Probabilistic analysis of wind turbine performance degradation due to blade erosion accounting for uncertainty of damage geometry. *Renewable and Sustainable Energy Reviews* **2023**, *178*, 113254.

20. Herring, R.; Dyer, K.; Martin, F.; Ward, C. The increasing importance of leading edge erosion and a review of existing protection solutions. *Renewable and Sustainable Energy Reviews* **2019**, *115*, doi: 10.1016/j.rser.2019.109382.
21. Wiser, R.; Jenni, K.; Seel, J.; Baker, E.; Hand, M.; Lantz, E.; Smith, A. Expert elicitation survey on future wind energy costs. *Nature Energy* **2016**, *1*, 16135, doi:10.1038/nenergy.2016.135.
22. Mishnaevsky Jr., L.; Thomsen, K. Costs of repair of wind turbine blades: Influence of technology aspects. *Wind Energy* **2020**, *23*, 2247-2255, doi:10.1002/we.2552.
23. Pryor, S.C.; Barthelmie, R.J.; Shepherd, T.J. Wind power production from very large offshore wind farms. *Joule* **2021**, *5*, 2663-2686, doi:10.1016/j.joule.2021.09.002.
24. Maniaci, D.C.; Westergaard, C.; Hsieh, A.; Paquette, J.A. Uncertainty quantification of leading edge erosion impacts on wind turbine performance. In Proceedings of the Journal of physics: Conference series, 2020; p. 052082.
25. Shankar Verma, A.; Jiang, Z.; Ren, Z.; Hu, W.; Teuwen, J.J. Effects of onshore and offshore environmental parameters on the leading edge erosion of wind turbine blades: A comparative study. *Journal of Offshore Mechanics and Arctic Engineering* **2021**, *143*, 042001.
26. McMorland, J.; Flannigan, C.; Carroll, J.; Collu, M.; McMillan, D.; Leithead, W.; Coraddu, A. A review of operations and maintenance modelling with considerations for novel wind turbine concepts. *Renewable and Sustainable Energy Reviews* **2022**, *165*, 112581.
27. Zahle, F.; Barlas, T.; Lonbaek, K.; Bortolotti, P.; Zalkind, D.; Wang, L.; Labuschagne, C.; Sethuraman, L.; Barter, G. *Definition of the IEA Wind 22-Megawatt Offshore Reference Wind Turbine*; Roskilde, Denmark: Technical University of Denmark (DTU): United States, 2024; p. Medium: ED; Size: 69 p.
28. Shohag, M.A.S.; Hammel, E.C.; Olawale, D.O.; Okoli, O.I. Damage mitigation techniques in wind turbine blades: A review. *Wind Engineering* **2017**, *41*, 185-210.
29. Mishnaevsky Jr, L. Root causes and mechanisms of failure of wind turbine blades: Overview. *Materials* **2022**, *15*, 2959.
30. Mankins, J.C. *Technology readiness levels*; Available for download from: https://aiaa.kavi.com/apps/group_public/download.php/2212/TRLs_MankinsPaper_1995.pdf, 1995; p. 1995.
31. Mankins, J.C. Technology readiness assessments: A retrospective. *Acta Astronautica* **2009**, *65*, 1216-1223.
32. Keegan, M.H.; Nash, D.; Stack, M. On erosion issues associated with the leading edge of wind turbine blades. *Journal of Physics D: Applied Physics* **2013**, *46*, 383001.
33. Letson, F.; Barthelmie, R.J.; Pryor, S.C. RADAR-derived precipitation climatology for wind turbine blade leading edge erosion. *Wind Energy Science* **2020**, *5*, 331-347.
34. Visbech, J.; Göçmen, T.; Hasager, C.B.; Shkalov, H.; Handberg, M.; Nielsen, K.P. Introducing a data-driven approach to predict site-specific leading edge erosion. *Wind Energy Science* **2023**, *8*, 173-191.
35. Preece, C.M. *Treatise on Materials Science and Technology, Vol. 16. Erosion*; 1979; p. 450.
36. Slot, H.; Gelinck, E.; Rentrop, C.; van der Heide, E. Leading edge erosion of coated wind turbine blades: Review of coating life models. *Renewable Energy* **2015**, *80*, 837-848.
37. Zhu, X.; Fu, X.; Liu, L.; Xu, K.; Luo, G.; Zhao, Z.; Chen, W. Damage mechanism of composite laminates under multiple ice impacts at high velocity. *International Journal of Impact Engineering* **2022**, *168*, 104296.
38. Heymsfield, A.; Szakáll, M.; Jost, A.; Giammanco, I.; Wright, R. A comprehensive observational study of graupel and hail terminal velocity, mass flux, and kinetic energy. *Journal of the Atmospheric Sciences* **2018**, *75*, 3861-3885.
39. Macdonald, J.; Stack, M. Some thoughts on modelling hail impact on surfaces. *Journal of Bio-and Tribo-Corrosion* **2021**, *7*, 1-7m doi: 10.1007/s40735-40020-00458-40734.
40. Kim, H.; Kedward, K.T. Modeling hail ice impacts and predicting impact damage initiation in composite structures. *AIAA journal* **2000**, *38*, 1278-1288.
41. Savana, R. Effect of Hail Impact on Leading Edge Polyurethane Composites. TUDelft, Available from http://repository.tudelft.nl/. 2022.
42. Hannesdóttir, Á.; Kral, S.T.; Reuder, J.; Hasager, C.B. Rain erosion atlas for wind turbine blades based on ERA5 and NORA3 for Scandinavia. *Results in Engineering* **2024**, *22*, 102010.
43. Dolan, B.; Fuchs, B.; Rutledge, S.; Barnes, E.; Thompson, E. Primary modes of global drop size distributions. *Journal of the Atmospheric Sciences* **2018**, *75*, 1453-1476.

44. Mayer, P.; Lubecki, M.; Stosiak, M.; Robakowska, M. Effects of surface preparation on the adhesion of UV-aged polyurethane coatings. *International Journal of Adhesion and Adhesives* **2022**, *117*, 103183.
45. Godfrey, M.; Siederer, O.; Zekonyte, J.; Barbaros, I.; Wood, R. The effect of temperature on the erosion of polyurethane coatings for wind turbine leading edge protection. *Wear* **2021**, *476*, 203720.
46. Lachenal, X.; Daynes, S.; Weaver, P.M. Review of morphing concepts and materials for wind turbine blade applications. *Wind energy* **2013**, *16*, 283-307.
47. Wan, D.; Chen, S.; Li, D.; Zhen, Q.; Zhang, B. Sand-Laden Wind Erosion Pair Experimental Analysis of Aerodynamic Performance of the Wind Turbine Blades. *Energies* **2024**, *17*, 2279.
48. Alajmi, A.F.; Ramulu, M. Characterization of the Leading-Edge Erosion of Wind Turbine Blades by Sand Particles Impingement. In Proceedings of the ASME International Mechanical Engineering Congress and Exposition, 2021; p. V08BT08A033.
49. Vinnes, M.K.; Hearst, R.J. Aerodynamics of an airfoil with leading-edge icing. *Wind Energy* **2021**, *24*, 795-811.
50. Rempel, L. Rotor blade leading edge erosion-real life experiences. *Wind Systems Magazine* **2012**, *11*, 22-24.
51. Amirat, Y.; Benbouzid, M.E.H.; Al-Ahmar, E.; Bensaker, B.; Turri, S. A brief status on condition monitoring and fault diagnosis in wind energy conversion systems. *Renewable and sustainable energy reviews* **2009**, *13*, 2629-2636.
52. Song, X.; Xing, Z.; Jia, Y.; Song, X.; Cai, C.; Zhang, Y.; Wang, Z.; Guo, J.; Li, Q. Review on the damage and fault diagnosis of wind turbine blades in the germination stage. *Energies* **2022**, *15*, 7492.
53. Lopez, J.C.; Kolios, A. An autonomous decision-making agent for offshore wind turbine blades under leading edge erosion. *Renewable Energy* **2024**, *227*, 120525.
54. Kong, K.; Dyer, K.; Payne, C.; Hamerton, I.; Weaver, P.M. Progress and trends in damage detection methods, maintenance, and data-driven monitoring of wind turbine blades–A review. *Renewable Energy Focus* **2023**, *44*, 390-412.
55. Cao, Z.; Li, S.; Li, C.; Li, P.; Ko, T.J. Formation mechanism and detection and evaluation methods as well as repair technology of crack damage in fiber-reinforced composite wind turbine blade: a review. *The International Journal of Advanced Manufacturing Technology* **2022**, *120*, 5649-5672.
56. Yan, Y.; Cheng, L.; Wu, Z.; Yam, L. Development in vibration-based structural damage detection technique. *Mechanical systems and signal processing* **2007**, *21*, 2198-2211.
57. Juengert, A.; Grosse, C.U. Inspection techniques for wind turbine blades using ultrasound and sound waves. In Proceedings of the Proceedings of the confernec eon Non-Destructive Testing in Civil Engineering: NDTCE, Nantes, France, 2009; p. 8pp.
58. Van Dam, J.; Bond, L.J. Acoustic emission monitoring of wind turbine blades. In Proceedings of the Smart Materials and Nondestructive Evaluation for Energy Systems 2015, 2015; pp. 55-69.
59. Xu, D.; Wen, C.; Liu, J. Wind turbine blade surface inspection based on deep learning and UAV-taken images. *Journal of Renewable and Sustainable Energy* **2019**, *11*, 053305.
60. Sørensen, B.F.; Lading, L.; Sendrup, P. *Fundamentals for remote structural health monitoring of wind turbine blades-a pre-project*; Risoe National Laboratory, Report # RISO-R-1336(EN): Report available from : https://www.osti.gov/etdeweb/biblio/20273791, 2002; p. 37 pp.
61. Shihavuddin, A.; Chen, X.; Fedorov, V.; Nymark Christensen, A.; Andre Brogaard Riis, N.; Branner, K.; Bjorholm Dahl, A.; Reinhold Paulsen, R. Wind turbine surface damage detection by deep learning aided drone inspection analysis. *Energies* **2019**, *12*, 676.
62. Aird, J.A.; Barthelmie, R.J.; Pryor, S.C. Automated Quantification of Wind Turbine Blade Leading Edge Erosion from Field Images. *Energies* **2023**, *16*, 2820.
63. Mishnaevsky, L.; Branner, K.; Petersen, H.; Beauson, J.; McGugan, M.; Sørensen, B. Materials for wind turbine blades: an overview. *Materials* **2017**, *10*, 1285.
64. Brøndsted, P.; Lilholt, H.; Lystrup, A. Composite materials for wind power turbine blades. *Annu. Rev. Mater. Res.* **2005**, *35*, 505-538.
65. Fæster, S.; Johansen, N.F.J.; Mishnaevsky Jr, L.; Kusano, Y.; Bech, J.I.; Madsen, M.B. Rain erosion of wind turbine blades and the effect of air bubbles in the coatings. *Wind Energy* **2021**, *24*, 1071-1082.
66. Hoksbergen, N.; Akkerman, R.; Baran, I. The Springer model for lifetime prediction of wind turbine blade leading edge protection systems: A review and sensitivity study. *Materials* **2022**, *15*, 1170.

67. Cortés, E.; Sánchez, F.; O'Carroll, A.; Madramany, B.; Hardiman, M.; Young, T.M. On the Material Characterisation of Wind Turbine Blade Coatings. *Materials* **2017**, *10*, 1146.
68. Eisenberg, D.; Laustsen, S.; Stege, J. Wind turbine blade coating leading edge rain erosion model: Development and validation. *Wind Energy* **2018**, *21*, 942-951.
69. Traphan, D.; Herráez, I.; Meinlschmidt, P.; Schlüter, F.; Peinke, J.; Gülker, G. Remote surface damage detection on rotor blades of operating wind turbines by means of infrared thermography. *Wind Energy Science* **2018**, *3*, 639-650.
70. Verma, A.S.; Castro, S.G.; Jiang, Z.; Teuwen, J.J. Numerical investigation of rain droplet impact on offshore wind turbine blades under different rainfall conditions: A parametric study. *Composite Structures* **2020**, *241*, 112096.
71. Nash, D.; Leishman, G.; Mackie, C.; Dyer, K.; Yang, L. A staged approach to erosion analysis of wind turbine blade coatings. *Coatings* **2021**, *11*, 681.
72. Castorrini, A.; Venturini, P.; Bonfiglioli, A. Generation of Surface Maps of Erosion Resistance for Wind Turbine Blades under Rain Flows. *Energies* **2022**, *15*, 5593.
73. Springer, G.S. *Erosion by liquid impact*; John Wiley and Sons,New York, NY: United States, 1976; p. 278.
74. Springer, G.S.; Yang, C.-I.; Larsen, P.S. Analysis of rain erosion of coated materials. *Journal of Composite Materials* **1974**, *8*, 229-252.
75. Herring, R.; Domenech, L.; Renau, J.; Šakalytė, A.; Ward, C.; Dyer, K.; Sánchez, F. Assessment of a wind turbine blade erosion lifetime prediction model with industrial protection materials and testing methods. *Coatings* **2021**, *11*, 767.
76. Maniaci, D.C.; MacDonald, H.; Paquette, J.; Clarke, R. *Leading Edge Erosion Classification System. Technical report from IEA Wind Task 46 Erosion of wind turbine blades*; Technical report from IEA Wind Task 46 Erosion of wind turbine blades. , 2022; pp. 52, Available from: https://iea-wind.org/task46/t46-results/.
77. Panthi, K.; Iungo, G.V. Quantification of wind turbine energy loss due to leading-edge erosion through infrared-camera imaging, numerical simulations, and assessment against SCADA and meteorological data. *Wind Energy* **2023**, *26*, 266-282.
78. Saenz, E.; Mendez, B.; Muñoz, A. Effect of erosion morphology on wind turbine production losses. In Proceedings of the Journal of Physics: Conference Series, 2022; p. 032059.
79. Bak, C. A simple model to predict the energy loss due to leading edge roughness. In Proceedings of the Journal of Physics: Conference Series, 2022; p. 032038.
80. Özçakmak, Ö.S.; Bretos, D.; Méndez, B.; Bak, C. Determination of annual energy production loss due to erosion on wind turbine blades. In Proceedings of the Journal of Physics: Conference Series, 2024; p. 022066.
81. Gaertner, E.; Rinker, J.; Sethuraman, L.; Zahle, Z.; Anderson, B.; Barter, G.; Abbas, B.; Meng, F.; Bortolotti, F.; Skrzypinski, W.; et al. *Definition of the IEA 15-Megawatt Offshore Reference Wind Turbine*; National Renewable Energy Laboratory: Golden, CO. NREL/TP-5000-75698. Available for download from: https://www.nrel.gov/docs/fy20osti/75698.pdf, 2020.
82. Malik, T.H.; Bak, C. Challenges in Detecting Wind Turbine Power Loss: The Effects of Blade Erosion, Turbulence and Time Averaging. *Wind Energy Science Discussions* **2024**, *2024*, 1-23.
83. Han, W.; Kim, J.; Kim, B. Effects of contamination and erosion at the leading edge of blade tip airfoils on the annual energy production of wind turbines. *Renewable energy* **2018**, *115*, 817-823.
84. Mishnaevsky Jr, L.; Tempelis, A.; Kuthe, N.; Mahajan, P. Recent developments in the protection of wind turbine blades against leading edge erosion: Materials solutions and predictive modelling. *Renewable Energy* **2023**, 118966.
85. Verma, A.S.; Yan, J.; Hu, W.; Jiang, Z.; Shi, W.; Teuwen, J.J. A review of impact loads on composite wind turbine blades: impact threats and classification. *Renewable and Sustainable Energy Reviews* **2023**, *178*, 113261.
86. Dashtkar, A.; Johansen, N.F.-J.; Mishnaevsky Jr, L.; Williams, N.A.; Hasan, S.W.; Wadi, V.S.; Silvello, A.; Hadavinia, H. Graphene/sol–gel modified polyurethane coating for wind turbine blade leading edge protection: Properties and performance. *Polymers and Polymer Composites* **2022**, *30*, 09673911221074197.
87. Major, D.; Palacios, J.; Maughmer, M.; Schmitz, S. Aerodynamics of leading-edge protection tapes for wind turbine blades. *Wind Engineering* **2021**, *45*, 1296-1316.

88. Kyle, R.; Wang, F.; Forbes, B. The effect of a leading edge erosion shield on the aerodynamic performance of a wind turbine blade. *Wind Energy* **2020**, *23*, 953-966.
89. Bera, P.; Lakshmi, R.; Pathak, S.M.; Bonu, V.; Mishnaevsky Jr, L.; Barshilia, H.C. Recent Progress in the Development and Evaluation of Rain and Solid Particle Erosion Resistant Coatings for Leading Edge Protection of Wind Turbine Blades. *Polymer Reviews* **2024**, *64*, 639-689.
90. Jones, S.M.; Rehfeld, N.; Schreiner, C.; Dyer, K. The Development of a Novel Thin Film Test Method to Evaluate the Rain Erosion Resistance of Polyaspartate-Based Leading Edge Protection Coatings. *Coatings* **2023**, *13*, 1849.
91. Verma, A.S.; Noi, S.D.; Ren, Z.; Jiang, Z.; Teuwen, J.J. Minimum leading edge protection application length to combat rain-induced erosion of wind turbine blades. *Energies* **2021**, *14*, 1629.
92. Ansari, Q.M.; Sánchez, F.; Mishnaevsky Jr, L.; Young, T.M. Evaluation of offshore wind turbine blades coating thickness effect on leading edge protection system subject to rain erosion. *Renewable Energy* **2024**, *226*, 120378.
93. Sareen, A.; Sapre, C.A.; Selig, M.S. Effects of leading edge erosion on wind turbine blade performance. *Wind Energy* **2014**, *17*, 1531-1542.
94. Katsivalis, I.; Chanteli, A.; Finnegan, W.; Young, T.M. Mechanical and interfacial characterisation of leading-edge protection materials for wind turbine blade applications. *Wind Energy* **2022**, *25*, 1758-1774.
95. Letson, F.; Pryor, S.C. From Hydrometeor Size Distribution Measurements to Projections of Wind Turbine Blade Leading Edge Erosion. *Energies* **2023**, *5*, 3906 doi: 3910.3390/en16093906.
96. Mishnaevsky Jr, L.; Thomsen, K. Costs of repair of wind turbine blades: Influence of technology aspects. *Wind Energy* **2020**, *23*, 2247-2255.
97. Skrzypiński, W.; Bech, J.; Hasager, C.B.; Tilg, A.; Bak, F.; Ch, V. Optimization of the erosion-safe operation of the IEA Wind 15 MW Reference Wind Turbine. *Journal of Physics: Conference Series* **2020**, *1618*, 052034, doi: 052010.051088/051742-056596/051618/052035/052034.
98. Visbech, J.; Göçmen, T.; Réthoré, P.-E.; Hasager, C.B. Erosion-safe operation using double deep Q-learning. In Proceedings of the Journal of Physics: Conference Series, 2024; p. 032047.
99. Oliver, T.J.; Nowlen, S.P. *A Phenomena Identification and Ranking Table (PIRT) Exercise for Nuclear Power Plant Fire Modeling Applications*; Sandia National Laboratory, Report # NUREG/CR-6978: 2008; p. 441.
100. Singh, P.M.; Chan, K.J.; Deo, C.S.; Deodeshmukh, V.; Keiser, J.R.; Ren, W.; Sham, T.; Wilson, D.F.; Yoder, G.; Zhang, J. Phenomena Identification and Ranking Table (PIRT) study for metallic structural materials for advanced High-Temperature reactor. *Annals of Nuclear Energy* **2019**, *123*, 222-229.
101. Maniaci, D.C.; Naughton, J.W. *V&V integrated program planning for wind plant performance*; Sandia National Lab.(SNL-NM), Albuquerque, NM (United States); Univ. of …: 2019.
102. Klaas-Witt, T.; Emeis, S. The five main influencing factors for lidar errors in complex terrain. *Wind Energy Science* **2022**, *7*, 413-431.
103. Wagner, R.; Pedersen, T.F.; Courtney, M.; Antoniou, I.; Davoust, S.; Rivera, R.L. Power curve measurement with a nacelle mounted lidar. *Wind Energy* **2014**, *17*, 1441-1453, doi:10.1002/we.1643.
104. Haupt, S.E.; Kosovic, B.; Shaw, W.; Berg, L.K.; Churchfield, M.; Cline, J.; Draxl, C.; Ennis, B.; Koo, E.; Kotamarthi, R. On bridging a modeling scale gap: Mesoscale to microscale coupling for wind energy. *Bulletin of the American Meteorological Society* **2019**, *100*, 2533-2550.
105. Prieto, R.; Karlsson, T. A model to estimate the effect of variables causing erosion in wind turbine blades. *Wind Energy* **2021**, *24*, 1031-1044.
106. Lochbihler, K.; Lenderink, G.; Siebesma, A.P. The spatial extent of rainfall events and its relation to precipitation scaling. *Geophysical Research Letters* **2017**, *44*, 8629-8636.
107. Kopp, J.; Manzato, A.; Hering, A.; Germann, U.; Martius, O. How observations from automatic hail sensors in Switzerland shed light on local hailfall duration and compare with hailpads measurements. *Atmospheric Measurement Techniques* **2023**, *16*, 3487–3503.
108. Lanza, L.G.; Cauteruccio, A.; Stagnaro, M. Rain gauge measurements. In *Rainfall*; Elsevier: 2022; pp. 77-108.
109. Pruppacher, H.R.; Beard, K. A wind tunnel investigation of the internal circulation and shape of water drops falling at terminal velocity in air. *Quarterly Journal of the Royal Meteorological Society* **1970**, *96*, 247-256.
110. Ro, Y.; Chang, K.-H.; Hwang, H.; Kim, M.; Cha, J.-W.; Lee, C. Comparative study of rainfall measurement by optical disdrometer, tipping-bucket rain gauge, and weighing precipitation gauge. *Natural Hazards* **2024**, *120*, 2829-2845.

111. Méndez, B.; Saenz, E.; Pires, Ó.; Cantero, E.; Bech, J.; Polls, F.; Peinó, E.; Udina, M.; Garcia-Benadí, A. Experimental campaign for the characterization of precipitation in a complex terrain site using high resolution observations. In Proceedings of the Journal of Physics: Conference Series, 2024; p. 042016.
112. Gunn, R.; Kinzer, G.D. The terminal velocity of fall for water droplets in stagnant air. *Journal of Atmospheric Sciences* **1949**, *6*, 243-248.
113. Tokay, A.; Petersen, W.A.; Gatlin, P.; Wingo, M. Comparison of raindrop size distribution measurements by collocated disdrometers. *Journal of Atmospheric and Oceanic Technology* **2013**, *30*, 1672-1690.
114. Prein, A.; Rasmussen, R.; Wang, D.; Giangrande, S. Sensitivity of organized convective storms to model grid spacing in current and future climates. *Philosophical Transactions of the Royal Society A* **2021**, *379*, 20190546.
115. Fridlind, A.M.; Li, X.; Wu, D.; van Lier-Walqui, M.; Ackerman, A.S.; Tao, W.-K.; McFarquhar, G.M.; Wu, W.; Dong, X.; Wang, J. Derivation of aerosol profiles for MC3E convection studies and use in simulations of the 20 May squall line case. *Atmospheric Chemistry and Physics* **2017**, *17*, 5947-5972.
116. Hong, S.-Y.; Dudhia, J.; Chen, S.-H. A revised approach to ice microphysical processes for the bulk parameterization of clouds and precipitation. *Monthly Weather Review* **2004**, *132*, 103-120.
117. Morrison, H.; Curry, J.; Khvorostyanov, V. A new double-moment microphysics parameterization for application in cloud and climate models. Part I: Description. *Journal of the Atmospheric Sciences* **2005**, *62*, 1665-1677.
118. Milbrandt, J.; Yau, M. A multimoment bulk microphysics parameterization. Part II: A proposed three-moment closure and scheme description. . *Journal of the Atmospheric Sciences* **2005**, *62*, 3065-3081.
119. Milbrandt, J.A.; Yau, M.K. A Multimoment Bulk Microphysics Parameterization. Part I: Analysis of the Role of the Spectral Shape Parameter. *Journal of the Atmospheric Sciences* **2005**, *62*, 3051-3064, doi:10.1175/JAS3534.1.
120. Thompson, G.; Field, P.R.; Rasmussen, R.M.; Hall, W.D. Explicit forecasts of winter precipitation using an improved bulk microphysics scheme. Part II: Implementation of a new snow parameterization. *Monthly Weather Review* **2008**, *136*, 5095-5115.
121. Khain, A.; Beheng, K.; Heymsfield, A.; Korolev, A.; Krichak, S.; Levin, Z.; Pinsky, M.; Phillips, V.; Prabhakaran, T.; Teller, A. Representation of microphysical processes in cloud-resolving models: Spectral (bin) microphysics versus bulk parameterization. *Reviews of Geophysics* **2015**, *53*, 247-322.
122. Xue, L.; Fan, J.; Lebo, Z.J.; Wu, W.; Morrison, H.; Grabowski, W.W.; Chu, X.; Geresdi, I.; North, K.; Stenz, R. Idealized simulations of a squall line from the MC3E field campaign applying three bin microphysics schemes: Dynamic and thermodynamic structure. *Monthly Weather Review* **2017**, *145*, 4789-4812.
123. Fan, J.; Han, B.; Varble, A.; Morrison, H.; North, K.; Kollias, P.; Chen, B.; Dong, X.; Giangrande, S.E.; Khain, A. Cloud-resolving model intercomparison of an MC3E squall line case: Part I—Convective updrafts. *Journal of Geophysical Research: Atmospheres* **2017**, *122*, 9351-9378.
124. Yang, Q.; Zhang, S.; Dai, Q.; Zhuang, H. WRF Rainfall Modeling Post-Processing by Adaptive Parameterization of Raindrop Size Distribution: A Case Study on the United Kingdom. *Atmosphere* **2021**, *13*, 36.
125. Shpund, J.; Khain, A.; Lynn, B.; Fan, J.; Han, B.; Ryzhkov, A.; Snyder, J.; Dudhia, J.; Gill, D. Simulating a Mesoscale Convective System Using WRF With a New Spectral Bin Microphysics: 1: Hail vs Graupel. *Journal of Geophysical Research: Atmospheres* **2019**, *124*, 14072-14101, doi: 14010.11029/12019JD030576.
126. Collow, T.W.; Robock, A.; Wu, W. Influences of soil moisture and vegetation on convective precipitation forecasts over the United States Great Plains. *Journal of Geophysical Research: Atmospheres* **2014**, *119*, 9338-9358.
127. Pryor, S.C.; Letson, F.; Shepherd, T.J.; Barthelmie, R.J. Evaluation of WRF simulation of deep convection in the US Southern Great Plains. *Journal of Applied Meteorology and Climatology* **2023**, *62*, 41-62.
128. Zhou, X.; Letson, F.; Crippa, P.; Pryor, S.C. Urban effect on precipitation and deep convective systems over Dallas-Fort Worth. *Journal of Geophysical Research: Atmospheres* **2024**, *129*, e2023JD039972.
129. Zeng, X.; Alves, L.; Boucher, M.-A.; Cherchi, A.; DeMott, C.; Dimri, A.; Gettelman, A.; Hanna, E.; Horinouchi, T.; Huang, J. Global Precipitation Experiment-A New World Climate Research Programme Lighthouse Activity. *Bulletin of the American Meteorological Society* **2024**.
130. Yu, S.; Hannah, W.; Peng, L.; Lin, J.; Bhouri, M.A.; Gupta, R.; Lütjens, B.; Will, J.C.; Behrens, G.; Busecke, J. ClimSim: A large multi-scale dataset for hybrid physics-ML climate emulation. In Proceedings of the Proceedings of Advances in Neural Information Processing Systems, Conference: Advances in Neural Information Processing Systems 36 (NeurIPS 2023), New Orleans, December 2023, 2024; p. 14.

131. DNVGL. *DNV-RP-0171 Testing of rotor blade erosion protection systems*; Available for purchase from: https://www.dnv.com/energy/standards-guidelines/dnv-rp-0171-testing-of-rotor-blade-erosion-protection-systems/, 2018.
132. Bech, J.I.; Johansen, N.F.-J.; Madsen, M.B.; Hannesdóttir, Á.; Hasager, C.B. Experimental study on the effect of drop size in rain erosion test and on lifetime prediction of wind turbine blades. *Renewable Energy* **2022**, *197*, 776-789.
133. Márquez, F.P.G.; Chacón, A.M.P. A review of non-destructive testing on wind turbines blades. *Renewable Energy* **2020**, *161*, 998-1010.
134. Rizk, P.; Rizk, F.; Karganroudi, S.S.; Ilinca, A.; Younes, R.; Khoder, J. Advanced wind turbine blade inspection with hyperspectral imaging and 3D convolutional neural networks for damage detection. *Energy and AI* **2024**, *16*, 100366.
135. Forsting, A.M.; Olsen, A.; Sørensen, N.; Fischer, A.; Markussen, C.; Bak, C. An aerodynamic digital twin of real-world leading edge erosion: Acquisition, Generation and 3D CFD. In Proceedings of the Journal of Physics: Conference Series, 2024; p. 022021.
136. Hwang, S.; An, Y.-K.; Yang, J.; Sohn, H. Remote inspection of internal delamination in wind turbine blades using continuous line laser scanning thermography. *International Journal of Precision Engineering and Manufacturing-Green Technology* **2020**, *7*, 699-712.
137. Ding, K.; Wu, C.; Luo, M.; Su, Z.; Ding, H.; Ye, Y.; Zhang, D. Surface Profile Inspection for Large Structures with Laser Scanning. *Surface Topography: Metrology and Properties* **2024**, *10.1088/2051-672X/ad7523*.
138. Leishman, G.; Nash, D.; Yang, L.; Dyer, K. A novel approach for wind turbine blade erosion characterization: an investigation using surface gloss measurement. *Coatings* **2022**, *12*, 928.
139. Zhang, Y.; Avallone, F.; Watson, S. Leading edge erosion detection for a wind turbine blade using far-field aerodynamic noise. *Applied Acoustics* **2023**, *207*, 109365.
140. Pugh, K.; Rasool, G.; Stack, M.M. Raindrop erosion of composite materials: some views on the effect of bending stress on erosion mechanisms. *Journal of Bio-and Tribo-Corrosion* **2019**, *5*, doi: 10.1007/s40735-40019-40234-40738.
141. Verma, A.S.; Wu, C.-Y.; Díaz, M.A.; Teuwen, J.J. Analyzing rain erosion using a Pulsating Jet Erosion Tester (PJET): Effect of droplet impact frequencies and dry intervals on incubation times. *Wear* **2024**, 205614.
142. Castorrini, A.; Barnabei, V.F.; Domenech, L.; Šakalyté, A.; Sánchez, F.; Campobasso, M.S. Impact of meteorological data factors and material characterization method on the predictions of leading edge erosion of wind turbine blades. *Renewable Energy* **2024**, *227*, 120549.
143. Hassani-Gangaraj, M.; Veysset, D.; Nelson, K.A.; Schuh, C.A. Melt-driven erosion in microparticle impact. *Nature Communications* **2018**, *9*, 5077, doi: 5010.1038/s41467-41018-07509-y.
144. Tempelis, A.; Mishnaevsky Jr, L. Surface roughness evolution of wind turbine blade subject to rain erosion. *Materials & Design* **2023**, *231*, 112011.
145. Reichert, P.; White, G.; Bayarri, M.J.; Pitman, E.B. Mechanism-based emulation of dynamic simulation models: Concept and application in hydrology. *Computational Statistics & Data Analysis* **2011**, *55*, 1638-1655.
146. Cappugi, L.; Castorrini, A.; Bonfiglioli, A.; Minisci, E.; Campobasso, M.S. Machine learning-enabled prediction of wind turbine energy yield losses due to general blade leading edge erosion. *Energy Conversion and Management* **2021**, *245*, 114567.
147. Campobasso, M.S.; Castorrini, A.; Cappugi, L.; Bonfiglioli, A. Experimentally validated three-dimensional computational aerodynamics of wind turbine blade sections featuring leading edge erosion cavities. *Wind Energy* **2022**, *25*, 168-189.
148. Nikuradse, J. *Laws of flow in rough pipes*; Technical Memorandum NASA TM 1292, Lewis Research Center, Washington, USA: Available for download from: https://digital.library.unt.edu/ark%3A/67531/metadc63009/m2/1/high_res_d/19930093938.pdf, 1950.
149. Kadivar, M.; Tormey, D.; McGranaghan, G. A review on turbulent flow over rough surfaces: Fundamentals and theories. *International Journal of Thermofluids* **2021**, *10*, 100077.
150. Castorrini, A.; Ortolani, A.; Campobasso, M.S. Assessing the progression of wind turbine energy yield losses due to blade erosion by resolving damage geometries from lab tests and field observations. *Renewable Energy* **2023**, *218*, 119256.

151. Castorrini, A.; Ortolani, A.; Minisci, E.; Campobasso, M. Opensource machine learning metamodels for assessing blade performance impairment due to general leading edge degradation. In Proceedings of the Journal of Physics: Conference Series, 2024; p. 052055.
152. Barthelmie, R.J.; Doubrawa, P.; Wang, H.; Giroux, G.; Pryor, S.C. Effects of an escarpment on flow parameters of relevance to wind turbines. *Wind Energy* **2016**, *19*, 2271-2286.
153. Latiffianti, E.; Ding, Y.; Sheng, S.; Williams, L.; Morshedizadeh, M.; Rodgers, M. Analysis of leading edge protection application on wind turbine performance through energy and power decomposition approaches. *Wind Energy* **2022**, *25*, 1203-1221.
154. Technical University of Denmark. Preventing MIcroplastics pollution in SEa water from offshore wind (PREMISE) project. https://premise.dtu.dk/. Available online: (accessed on 1 October 2024).
155. Thacker, B.H.; Doebling, S.W.; Hemez, F.M.; Anderson, M.C.; Pepin, J.E.; Rodriguez, E.A. *Concepts of model verification and validation*; Los Alamos National Laboratory, Report # LA-14167-MS: California, 2004; p. 41.